SIMULATION OF 16MO3 STEEL USED IN BOILERS

Lappeenranta–Lahti University of Technology LUT

Master's Programme in Mechanical Engineering, Master's thesis

2025

Kimmo Hakala

Examiners: Associate Professor Hemantha Yeddu

Jiayi Chen, D.Sc. (Tech.)

ABSTRACT

Lappeenranta–Lahti University of Technology LUT

LUT School of Energy Systems

Mechanical Engineering

Kimmo Hakala

Simulation of 16MO3 steel used in boilers

Master's thesis

2025

76 pages, 26 figures, 9 table and 4 appendices

Examiners: Associate Professor Hemantha Yeddu and Jiayi Chen, D.Sc. (Tech.)

Keywords: 16Mo3 steel, Boiler, Welding, Repair welds, Heat-affected zone (HAZ), Grain growth, Creep, Crack propagation, Failure mechanisms, High-temperature steel, CHP boiler, Microstructure, Steel alloying, Preheating, Post-weld heat treatment (PWHT), Corrosion, Fatigue, Thermal stress

This study investigates failure mechanisms in CHP power boilers after repair welding, with a focus on deformation from pre-existing defects. Using MatCalc simulations, microstructural changes in the heat-affected zone (HAZ), particularly grain growth, are analyzed. Emphasis is placed on 16Mo3 steel, commonly used in boiler tubes. The research examines material behavior, failure probability, and the effects of heat treatment on mechanical properties. Coarse grain growth in welds reduces toughness and increases crack susceptibility, while fine grains enhance performance.

TIIVISTELMÄ

Lappeenrannan–Lahden teknillinen yliopisto LUT

LUTin energiajärjestelmien tiedekunta

Konetekniikka

Kimmo Hakala

16Mo3-teräksen simulointi kattilakäytössä

Konetekniikan diplomityö

2025

76 sivua, 26 kuvaa, 9 taulukkoa ja 4 liite

Arvostelijat: Apulaisprofessori Hemantha Yeddu ja Jiayi Chen, TkT

Avainsanat: 16Mo3-teräs, kattila, hitsaus, korjaushitsaus, lämpövaikutusalue (HAZ), raekoon kasvu, viruminen, halkeamien eteneminen, vauriomekanismit, korkealämpöteräs, CHP-kattila, mikrorakenne, teräksen seostus, esilämmitys, hitsauksen jälkeinen lämpökäsittely (PWHT), korroosio, väsymislujuus, lämpöjännitys

Tässä tutkimuksessa tarkastellaan voimalaitoskattiloiden vauriomekanismeja korjaushitsauksen jälkeen, erityisesti alkuperäisten vikojen aiheuttamia muodonmuutoksia teoreettisella tasolla. MatCalc-ohjelmistolla simuloidaan mikrotason ilmiöitä lämpövaikutusalueella (HAZ), painottaen raerakenteen vaikutusta materiaalin käyttäytymiseen. Tutkimus keskittyy 16Mo3-teräkseen, jota käytetään yleisesti kattilaputkistoissa, ja rajautuu CHP-voimaloihin. Työssä analysoidaan materiaalivalintojen ja lämpökäsittelyjen vaikutuksia teräksen mekaanisiin ominaisuuksiin sekä vaurioitumisriskeihin. Raekoon kasvu heikentää hitsien kestävyyttä vähentämällä lujuutta, sitkeyttä ja väsymislujuutta. Karkea raerakenne lisää haurauden, halkeamien etenemisen ja vetyhaurauden riskiä, kun taas hienorakeinen rakenne parantaa mekaanista suorituskykyä.

ACKNOWLEDGEMENTS

Thanks to Hemantha Yeddu, who gave me the subject for this final thesis.

The power plant had a significant issue at the boiler exhaust shaft connection area to the three cyclone connections, where multiple failures had occurred in the past. This phenomenon was the original focus of my thesis. However, due to the idea had to be adjusted so that the work could be completed without direct access to the power plant while ensuring that sensitive information was not publicly shared through the final thesis.

For helping and planning this thesis, I want to thank Hemantha Yeddu for all the support throughout this long and slow-progressing process, leading to its completion while I was simultaneously working on the VR locomotive project with Stadler as the locomotive supplier.

Additionally, many thanks to D.Sc. (Tech.) Jiayi Chen for reviewing the calculations and providing excellent guidance, suggestions, tips, and advice throughout the work. Your prompt responses and valuable support, especially toward the end of the thesis, greatly appreciated.

SYMBOLS AND ABBREVIATIONS

Symbols

C	Carbon
A1 / A3	Phase transformation temperatures in steels
Al	Aluminium
B	Boron
Ce(IIW)	Carbon equivalent (weldability formula)
Cr	Chromium
Cu	Copper
Fe-C	Iron-carbon equilibrium system
Mn	Manganese
Mo	Molybdenum
Ms	Martensite start temperature
N	Nitrogen
Ni	Nickel
P	Phosphorus
S	Sulphur
Si	Silicon
t8/5	Cooling time between 800°C and 500°C
Ti	Titanium
V	Vanadium

Abbreviations

16Mo3	A Specific Grade of Heat-Resistant Steel (EN 1.5415, DIN 15Mo3)
BCC	Body-Centered Cubic
CFB	Circulating Fluidized Bed
CGHAZ	Coarse Grain Heat-Affected Zone
CHP	Combined Heat and Power
DIN	Deutsches Institut für Normung (German Standards Institute)
EN	European Norm (European Standard)
FCC	Face-Centered Cubic
FGHAZ	Fine Grain Heat-Affected Zone
HAZ	Heat-Affected Zone
HCP	Hexagonal Close-Packed
ICHAZ	Intercritical Heat-Affected Zone
NDT	Non-Destructive Testing
PWHT	Post-Weld Heat Treatment
Rm	Tensile Strength
SCHAZ	Subcritical Heat-Affected Zone
TTT	Time-Temperature-Transformation (diagram)
WPS	Welding Procedure Specification
#CALC!	Normalized condition IIW International Institute of Welding

Table of contents

Abstract

Tiivistelmä

Acknowledgements

Symbols and abbreviations

1 Introduction 9
2 Background and motivation 10
2.1 Evolution of Steam Boilers and Safety Considerations 10
2.2 Steam Boiler Applications and Energy Sources 11
2.3 Operating Principle of a Steam Boiler 14
2.4 Research Objectives and Methodology 15
2.5 Research Questions 15
2.6 Research Methods 16
2.7 Scope 16
3 Literature review 17
3.1 Atomic Structure and Lattice Spacing in Iron Alloys 18
3.2 Heat Treatment of Steel 18
3.3 Alloying Elements in Steel 23
3.4 Materials for Boiler Components 24
3.5 Welding of Steel 26
3.6 Grain Size 30
3.7 High-strength steels 32
3.8 Studying the microstructure of metal 35
3.9 Weldability of High-Strength Steels 35
3.10 Failure mechanisms in power plant boilers 37
3.11 Properties of 16Mo3, EN 1.5415, DIN 15Mo3 Steel Used in the Boiler 44
3.12 Theoretical Possibilities 47
3.13 Design Curves in a Boiler 49
4 Simulation in welding processes 50

5 Metallurgical simulation.....52
6 Results 63
7 Discussion.....66
8 Conclusions 68
References.....70

Appendices

Appendix 1. Power-plant WPS for 16Mo3

1 Introduction

Power plant boilers are subjected to extreme operating conditions, including high temperatures, pressure variations, and thermal cycling, which contribute to the degradation of materials and structures over time. This study investigates the most common failure mechanisms in power plant boilers, with a particular emphasis on the heat-affected zone (HAZ) of repair welds. The research examines the metallurgical transformations occurring in the HAZ and their implications for material durability and structural integrity.

The thermal effects on power boiler components influence both their operational efficiency and long-term reliability. The simulation of grain growth in the HAZ provides a basis for understanding the impact of continuous repair welding on microstructural evolution.

This study employs computational simulations to analyse the metallurgical properties of repair welds in power plants. Special attention is given to the temperature conditions and at the interface between the boiling section of a circulating fluidized bed (CFB) boiler and its cyclones. The research aims to determine the primary causes of weld seam degradation in this region and to model similar failure mechanisms in other sections of power boilers.

The operating conditions of power boilers vary significantly depending on their purpose and manufacturing era. Future developments in the energy industry, influenced by technological innovations and regulatory decisions, will continue to shape the requirements for boiler materials and design. The presence of multiple stress-inducing factors complicates the prediction of material durability, making the study of damage mechanisms increasingly relevant.

2 Background and motivation

The analysis conducted in this study is grounded in a comprehensive synthesis of existing literature, peer-reviewed academic publications, technical standards, and prior research findings relevant to power plant boiler materials, welding techniques, and failure mechanisms. By integrating theoretical frameworks with empirical data from earlier studies, the research aims to build a solid foundation for understanding the metallurgical behaviour and structural performance of 16Mo3 steel under operating and repair conditions.

2.1 Evolution of Steam Boilers and Safety Considerations

Steam boilers have been integral to industrial development since the 18th century, playing a crucial role in the expansion of industries such as textiles. However, the introduction of steam-powered machinery also brought significant safety challenges, necessitating improvements in boiler design and manufacturing techniques. The transformation of water into steam at atmospheric pressure requires temperatures exceeding 100°C, resulting in a volumetric expansion of approximately 1,600 times its original state. This immense expansion potential made early steam boilers prone to catastrophic failures.

A pressure vessel is defined as a sealed container designed to store gases or liquids at pressures higher than atmospheric pressure. Due to the inherent risks associated with pressurized systems, stringent regulations govern the manufacturing, operation, and maintenance of pressure vessels. In the European Union, these regulations are outlined in the Pressure Equipment Directive (PED), which also serves as the foundation for Finnish pressure vessel legislation.

During the 19th-century industrialization, efforts to increase the efficiency of steam engines led to higher operating pressures, which, in turn, increased the frequency of boiler explosions. In the United States alone, more than 10,000 boiler explosions were recorded around the turn of the 20th century. To mitigate these risks, safety measures such as pressure relief valves were introduced, and insurance companies began enforcing stricter design standards. (Hakkarainen, 2013.)

By the early 20th century, advancements in material science, safety technology, and structural design significantly reduced the occurrence of boiler accidents. The use of high-strength steels and improved engineering practices further enhanced the reliability of steam boilers in industrial applications.

2.2 Steam Boiler Applications and Energy Sources

A steam boiler is a closed vessel in which water is heated to produce pressurized steam, which is then utilized in various industrial processes, including power generation, district heating, and mechanical work. Steam boilers are commonly integrated with heat exchangers, steam turbines, or steam engines, where they contribute to energy conversion processes.

The energy required for steam production is derived from various fuel sources, including coal, wood, oil, and alternative fuels such as Solid Recovered Fuel (SRF), natural gas, or industrial byproducts like bark sludge. The choice of fuel depends on the application, efficiency requirements, and environmental considerations. Additionally, renewable energy sources, such as solar and geothermal energy, are increasingly being explored for steam generation.

The efficiency of a conventional steam boiler typically ranges from 55% to 65%, depending on design parameters and operational conditions. However, advancements in boiler technology have enabled efficiencies approaching 100% under optimized conditions. Despite these improvements, modern material production often involves minimizing safety margins to reduce material usage and weight. As a result, contemporary boiler components are often designed with thinner materials, increasing the need for precise strength calculations and failure analysis.

Comparative studies of power plant infrastructure reveal that older steam pipelines were significantly thicker than those in newer installations. For instance, steam pipelines in power plants constructed in 1977 were several centimetres thicker than those in plants built in 1994. This suggests that earlier material designs provided higher safety margins, reducing the likelihood of crack formation and propagation.

As material optimization has led to reduced thickness and safety factors, research into failure mechanisms has gained increasing importance. On-site monitoring and predictive maintenance strategies have been developed to ensure the continued reliability of power plant components. These considerations form the basis of this study, which aims to contribute to the understanding of damage mechanisms in modern power plant boilers. (Souza & SpringerLink, 2012; Hakkarainen, 2013; Kalliokoski, 2013.)

The research focuses on power plants in Oulu, Finland, where extensive operational experience has been gained through the maintenance of three power plants and a hydropower facility in the region. A particular emphasis is placed on the exhaust duct and its theoretical behavior within a CFB boiler equipped with three cyclones and an intermediate-pressure turbine.

Throughout history, various boiler designs have been developed to accommodate different operational requirements. These include condensing power plants, natural circulation boilers, and forced circulation boilers as in figure 1. Each of these configurations presents unique challenges in terms of thermal stress distribution, material fatigue, and long-term durability.

By modelling the behaviour of weld seams in high-temperature environments, this research seeks to enhance the understanding of failure mechanisms in power plant boilers. The findings may contribute to the development of improved maintenance practices, material selection strategies, and predictive maintenance tools for industrial applications.

Give a brief introduction to what each chapter is about. Write at least two sentences under the chapter heading.

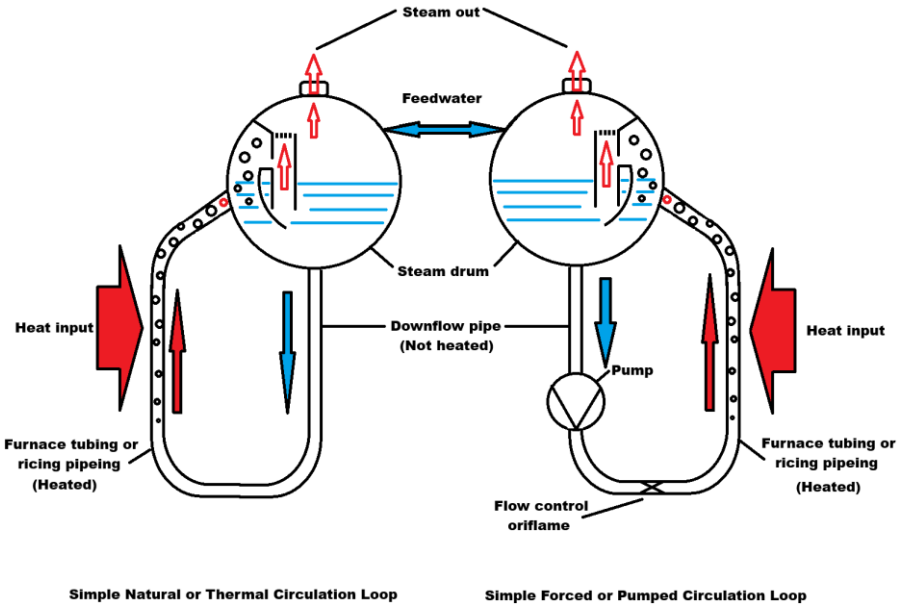

Figure 1. Naturally cycled boiler and forced circulation boiler principle

Today's boilers are mainly fixed grate burning boilers designed for different fuel applications as in figure 2. The circulating fluidized bed boiler (CFB) and cyclone boiler are the most common types used today.

To days boilers are mainly fixed grate burning boilers for different burning fuel applications. Circulating fluidised bed boiler and a cyclone (CFB) are most usual today, this can be seen in figure 3.

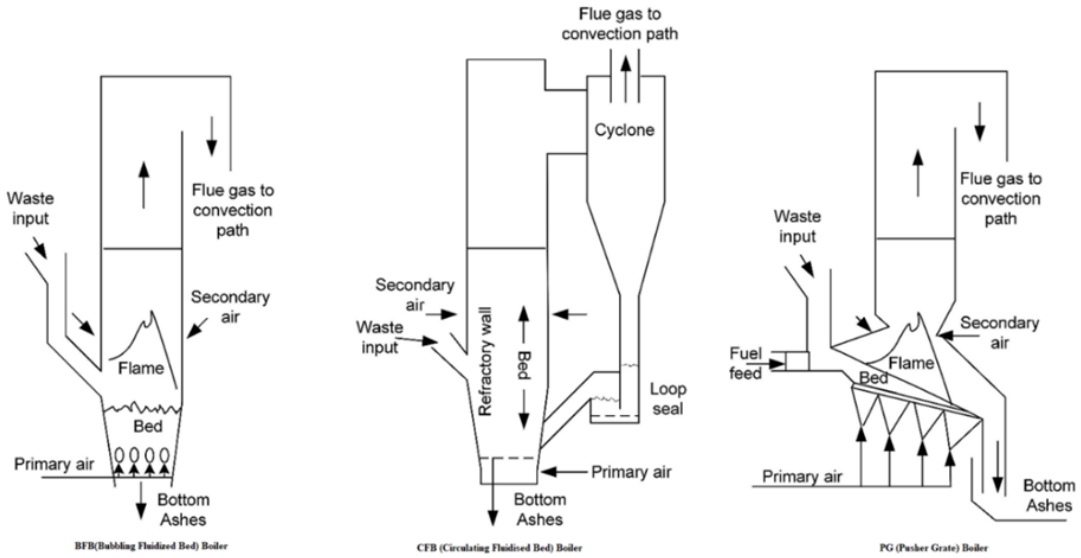

Figure 1. Different boiler bed grates (Leckner, Bo, and Fredrik Lind, 2020).

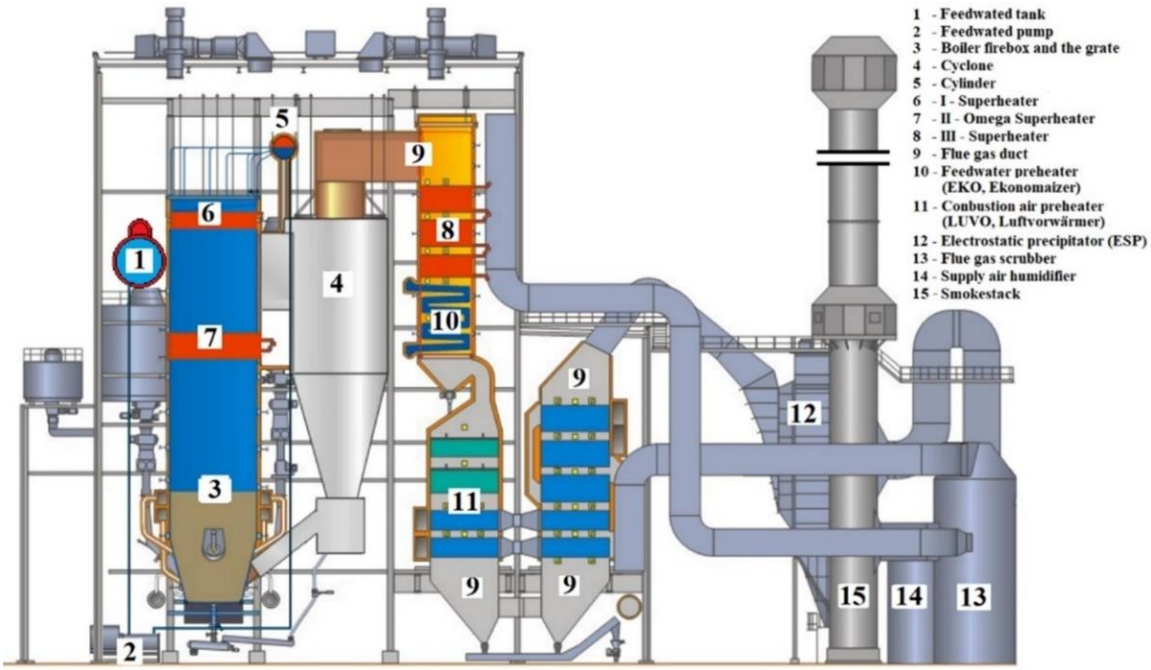

Figure 2. Circulating Fluidised Bed boiler (CFB) and its basic parts

2.3 Operating Principle of a Steam Boiler

A steam boiler converts water into steam through heat transfer, governed by thermodynamic principles. Structural support is designed to allow vertical thermal expansion, reducing stress within the flue gas duct.

Combustion and Firebox Operation - Fuel combusts on a firebox grate, generating high temperatures. Airflow carries sand and flue gases into cyclones, where sand is separated and recirculated. Refractory lining protects the firebox from thermal stress, while evaporative cooling by water in heat exchanger walls prevents overheating.

Firebox Wall Design - Wall structure varies by application, often incorporating masonry or coatings to mitigate erosion—especially in the lower sections exposed to intense wear.

Steam Generation and Feedwater Cycle - Feedwater is treated and preheated before entering the steam drum via high-pressure pumps. Inside the drum, steam and water separate by density. Automated control systems regulate water level and pressure, preventing conditions like dry boiling or over pressurization.

Superheating and Energy Conversion - Saturated steam is further heated in superheaters to increase pressure and energy output for turbines. Reheating of steam post-turbine improves efficiency. Superheater temperatures are limited to ~550°C due to material constraints.

Flue Gas Management - Flue gases pass through the economizer and exit via the chimney. Proper insulation prevents condensation and acid corrosion by maintaining temperatures above ~150°C.

Structural Integrity and Maintenance - Structural weaknesses commonly occur at weld seams, particularly in the heat-affected zones (HAZ) of repair welds. Defects arise from thermal cycling or inherent material flaws. Non-destructive testing (NDT) and visual inspections are critical. Steam leaks pose safety risks, especially if involving superheated steam, which may not be visually detectable. (Souza & SpringerLink, 2012; Hakkarainen, 2013; Kalliokoski, 2013.)

2.4 Research Objectives and Methodology

This study aims to investigate the primary causes of defects in boilers and assess factors influencing their reliability and lifespan. Additionally, the impact of repair welds on boiler frame strength is evaluated through simulation.

2.5 Research Questions

What are the most common causes of boiler defects?

How do operating conditions impact boiler reliability?

How do material properties affect boiler performance?

To what extent do repair welds influence boiler durability?

2.6 Research Methods

A comprehensive literature review is conducted to understand the behavior of metallic materials under different operating conditions. Additionally, a simulation is performed to evaluate the impact of repair welding on the HAZ region of boiler components.

2.7 Scope

The study focuses on simulating grain growth in repair welds of the commonly used boiler steel 16Mo3 (EN 1.5415, DIN 15Mo3). The research aims to quantify the degradation in the HAZ region due to multiple repairs and explore alternative boiler repair solutions.

3 Literature review

Lattice Structures - Metals consist of crystalline grains, ranging in size from 0.5μm to several millimetres. The mechanical properties of metals can be modified through heat treatments such as quenching, tempering, and annealing. Crystallographic structures are categorized into 14 lattice models, with the most relevant being FCC, Face-Cantered Cubic and BCC Body-Cantered Cubic and HCP Hexagonal Close-Packed structures, which dictate the material's mechanical performance and thermal stability. This structured and scientific revision improves readability, clarity, and accuracy while maintaining the technical integrity of the original text.

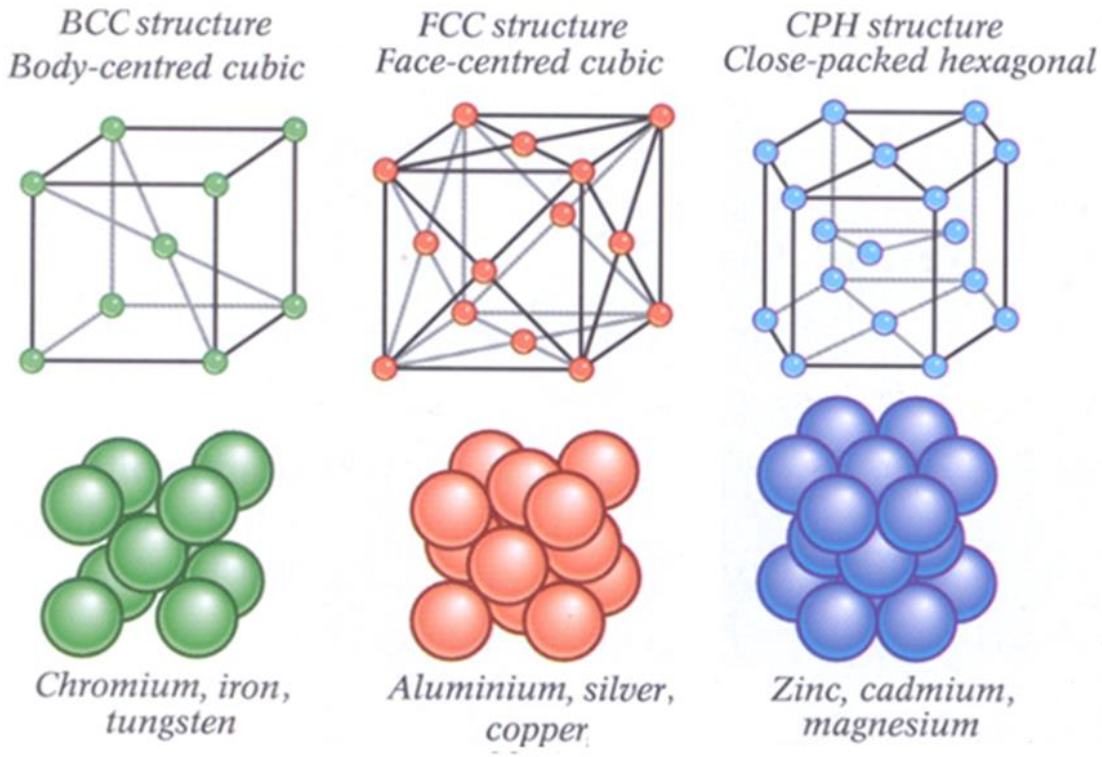

Figure 3. The most important lattice structures (Souza, Gilberto Francisco Martha de, and Springer Link, 2012).

3.1 Atomic Structure and Lattice Spacing in Iron Alloys

According to the literature, the atomic size of an alloying element that can fit into the interstitial sites of ferrite (α-iron) and the face-cantered cubic (FCC) lattice structure of δ-iron can reach up to 29.1% of the diameter of the lattice atom. In contrast, the FCC lattice of austenitic γ-iron provides a larger interstitial space, accommodating up to 41.4% of the diameter of a carbon atom. This increased lattice spacing in austenitic steel facilitates precipitation processes more readily than in ferritic or delta-phase iron structures (Souza, Gilberto Francisco Martha de, and Springer Link, 2012).

3.2 Heat Treatment of Steel

Allotropic ferritic carbon steel exhibits different phases and crystal structures depending on temperature. In microstructural analysis, these phases correspond to mixtures of various states, including austenite, ferrite, bainite, cementite, and other phase constituents. The heat treatment of steel, such as hardening or quenching, significantly alters its microstructure and mechanical properties due to phase transformations, which are a fundamental aspect of the material's allotropy.

The figure 5 below illustrates the phase transitions of carbon steel and the corresponding microstructural compositions as a function of temperature.

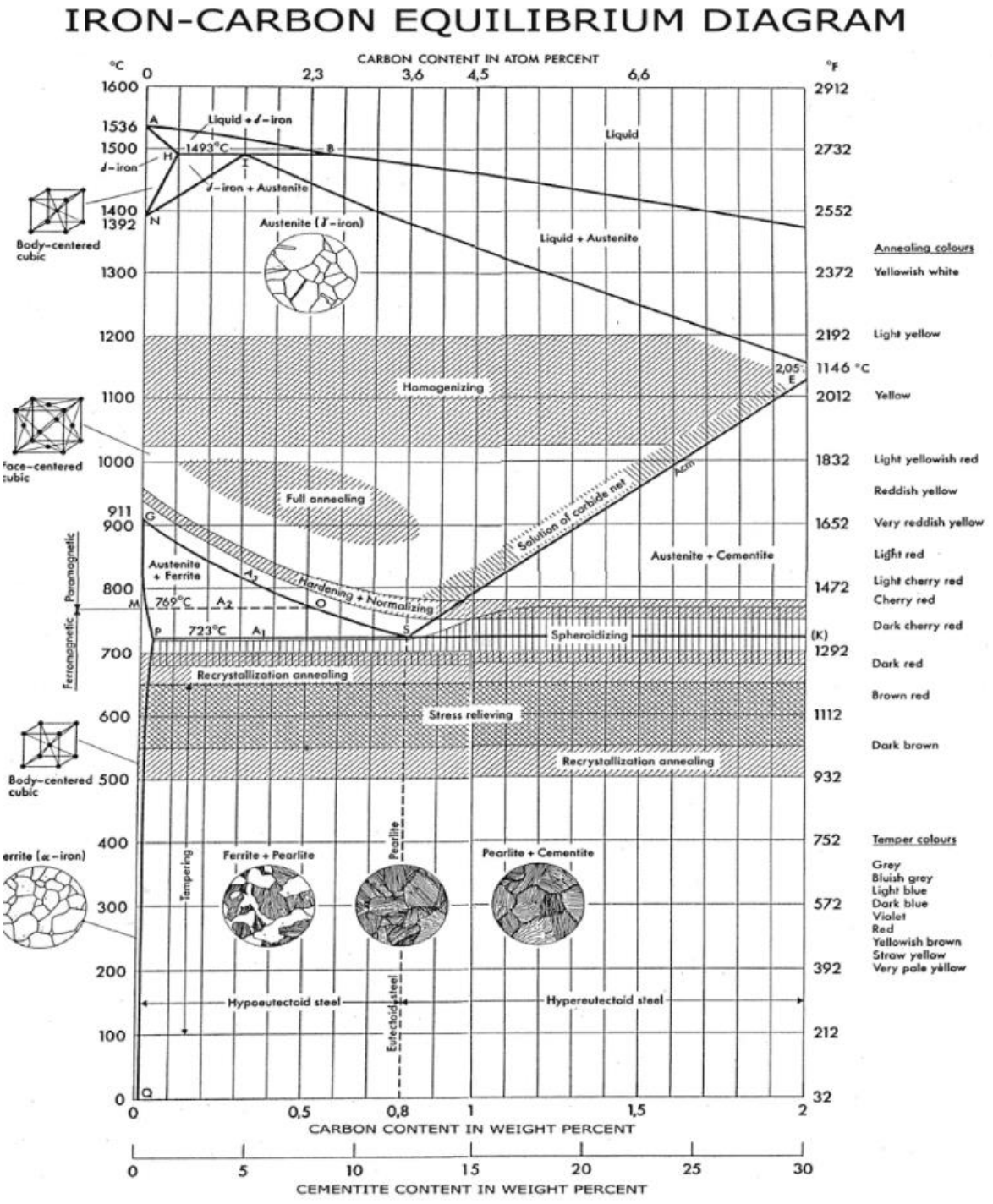

Figure 4. Iron-carbon Fe - C equilibrium diagram (Souza, Gilberto Francisco Martha de, and SpringerLink, 2012).

When carbon steel cools at a very slow rate, ferrite, pearlite, and their associated microstructures form. This transformation can be analysed using phase diagrams specific to the material. However, the traditional Fe-C phase diagram does not explicitly account for

the cooling rate, even though it provides information about the carbon content at different temperature ranges. The cooling rate plays a critical role in phase transformations, directly influencing the relative proportions of the resulting microstructures as austenite decomposes.

At a slow cooling rate, austenite begins to decompose into ferrite and pearlite at approximately 727°C. As the cooling rate increases, bainitic structures begin to form, leading to a transition region where bainite becomes the dominant phase. In cases of extremely rapid cooling—such as during quenching—the transformation results in a martensitic microstructure. Martensite formation significantly increases the hardness of steel due to its body-centred tetragonal (BCT) lattice structure, which introduces internal stresses.

During the hardening process, steel is first heated to the austenitic phase (above 723°C) and then rapidly cooled, often through immersion in water or oil. In carbon steels, the hardened layer typically extends only 3–4 mm from the surface, as cooling rates decrease with depth. High-alloy steels, in contrast, exhibit deeper hardening due to their enhanced thermal properties and alloying elements that delay phase transformations.

The S-curves (time-temperature-transformation, TTT diagrams) of steel are essential for predicting how austenite decomposes into ferrite, pearlite, bainite, or martensite under different cooling conditions. By cooling steel to a specific temperature after annealing and holding it at that temperature, the resulting microstructure—including the proportions of the different phases—can be determined using a static TTT diagram. This approach enables precise control over the material properties of steel. (Souza, Gilberto Francisco Martha de, and SpringerLink, 2012.)

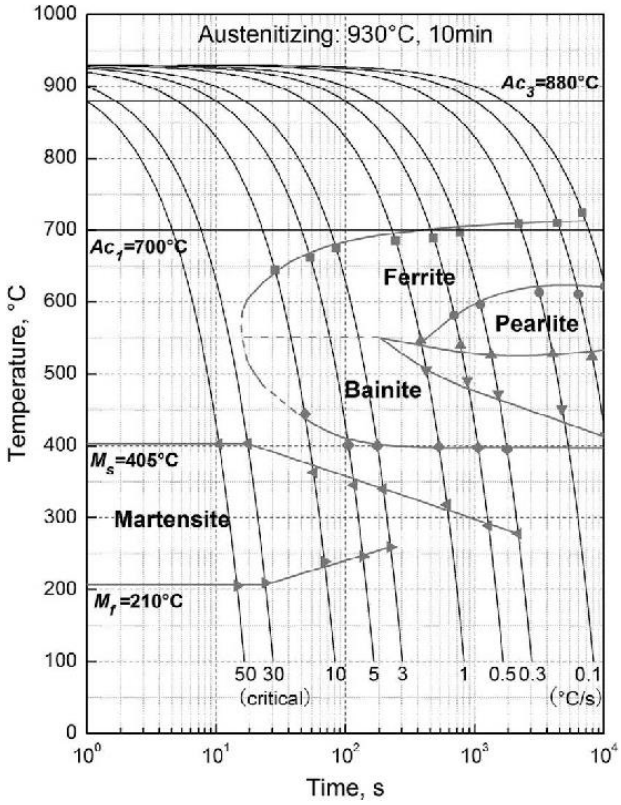

Figure 5. Iron-carbon TTT diagram (Shu ZHOU, Ke ZHANG, Nailu CHEN, Jianfeng and Yonghua RONG, 2011).

The diagram illustrates the phase composition of steel formed at various cooling rates and their corresponding hardness levels. For instance, steel with a hardness of 289 HV consists of 10% ferrite and 90% pearlite. As the cooling rate increases, the proportion of stronger and harder phases in the steel also increases. The Ms marking designates the temperature at which martensite begins to form.

In 0.8% carbon steel at 723°C, austenite initiates a transformation into ferrite within the material, accompanied by the formation of cementite. When the cooling process is sufficiently slow, pearlite develops. Pearlite, found in steels and cast irons, is characterized by alternating lamellae of ferrite and cementite. It represents the microstructure of a eutectoid mixture (0.8% carbon content) at room temperature and constitutes the fundamental structure of numerous structural steels. If the steel contains less than 0.8% carbon, larger ferritic regions form at the grain boundaries of pearlite, whereas a carbon content exceeding 0.8% results in an increased concentration of cementite (iron carbide). At ambient temperature, ferrite accommodates up to 0.02% carbon, while cementite contains

6.7% carbon. The ferrite present in pearlitic structures enhances ductility and malleability, whereas cementite contributes to increased strength and hardness. Consequently, steels used for blade manufacturing typically exhibit carbon content well above 0.8%. Carbon content directly influences steel's workability; hence, steels requiring high malleability tend to have relatively low carbon content.

Heat treatment consists of three distinct stages that influence the material's properties: (1) Heating, which involves elevating the temperature of the material based on its properties, dimensions, and shape; (2) Holding, where the material is maintained at a specified temperature until uniform thermal distribution is achieved; and (3) Cooling, often referred to as quenching, which solidifies the microstructural transformations. These processes impart specific mechanical characteristics to the material (Souza & SpringerLink, 2012).

Beyond tempering, normalization is another heat treatment process in which steel is heated near its austenitizing temperature, held until it reaches thermal equilibrium, and then allowed to cool in air. This process relieves internal stresses and refines the material structure. (Martikainen, 2015.)

One specialized heat treatment method is rejuvenation, achieved through controlled heating and holding, which homogenizes ferrite distribution within carbide inclusions. Post-hardening, steel exhibits extreme hardness and brittleness. To mitigate residual stresses, the material is heated almost immediately after hardening before undergoing subsequent machining processes. Hardening leads to martensitic transformation, which gradually transitions to spheroidal pearlite during subsequent heat treatments. The hardness reduction is contingent upon the tempering temperature and duration. Tempering temperatures can be estimated through oxidation-induced surface color variations.

An exemplary application of these principles is knife-making, a field in which practical experience has demonstrated that silver steel can be hardened in water or oil and then tempered at temperatures exceeding 200°C for several hours. This process, evident by a golden-yellow surface coloration, produces a chisel that retains its sharpness effectively. Stress relief improves material toughness and reduces brittleness by alleviating internal stresses. For instance, the typical tempering temperature for S355 steel ranges from 180–200°C, with tempering ceasing when the material is allowed to cool in air. (Souza & SpringerLink, 2012; Li et al., 2021.)

3.3 Alloying Elements in Steel

Steel is commonly alloyed with various elements to modify its properties based on its intended application. Alloying elements influence steel either indirectly, such as by altering phase transformation temperatures, or directly, by enhancing mechanical characteristics like impact resistance. By carefully combining different alloying elements, steel properties can be precisely tailored to meet manufacturing requirements (Souza & SpringerLink, 2012).

Carbon (C): The principal alloying element in steel, carbon significantly enhances martensite formation during hardening, leading to increased hardness and strength. However, excessive carbon content reduces weldability and ductility.

Nickel (Ni): Enhances strength, hardness, and corrosion resistance while stabilizing austenite and improving impact resistance.

Chromium (Cr): Increases corrosion resistance by forming a protective oxide layer, enhances wear resistance, and restricts austenite grain growth.

Manganese (Mn): Improves hardenability, impact strength, and wear resistance but may reduce toughness when present in excessive amounts.

Boron (B): Enhances hardenability in low-alloyed and unalloyed steels but can compromise impact resistance at high concentrations.

Aluminium (Al): Reduces grain size and improves impact resistance by binding nitrogen and oxygen.

Silicon (Si): Enhances work hardening and oxidation resistance but must be carefully controlled to avoid negative effects on cold forging.

Copper (Cu): Acts as an austenite stabilizer but may lead to hot rolling defects at concentrations above 0.2%.

Titanium (Ti): Refines grain structure and improves deformation resistance but can impair machinability when forming TiN inclusions.

Calcium (Ca): Improves machinability and extends tool life in machining applications.

Molybdenum (Mo): Enhances high-temperature strength and creep resistance, improving overall durability.

Tungsten (W): Increases hardness retention and tensile strength, especially in high-speed tool steels. (Martikainen, 2015)

3.4 Materials for Boiler Components

Boilers are primarily constructed using steel due to its superior mechanical properties. Boiler steels can be categorized into unalloyed and alloyed types, with alloying elements like chromium, nickel, and molybdenum enhancing their performance.

Pressure components in water-tube boilers must withstand high temperatures, stress fluctuations, and corrosion. Material selection is governed by standards such as SFS-EN 12952-2, which defines requirements for structural steel components, including seamless and welded pipes, castings, and fasteners. (Kalliokoski, 2013, Barbosa et al., 2012.)

At temperatures above 550°C, steel surfaces form protective oxide layers that inhibit further oxidation. High-temperature steels contain alloying elements like chromium, silicon, and aluminium to enhance oxidation resistance. Standards such as SFS-EN 10095 classify heat-resistant steels based on their microstructural composition. (Kalliokoski, 2013; Li et al., 2021.)

Ferritic steels maintain a ferritic microstructure across all temperature ranges due to their high chromium content. The incorporation of silicon and aluminium into these steels further enhances their resistance to flaking and improves the durability of the ferritic phase. These steels exhibit excellent resistance to sulphurous gases, such as those generated from peat combustion. However, their creep resistance at elevated temperatures is inferior to that of austenitic refractory steels. Ferritic steels are also susceptible to brittleness within certain temperature ranges. When exposed to temperatures exceeding 900°C, grain growth occurs, leading to structural embrittlement. Consequently, exposure to impact-like stresses should be minimized.

Ferritic-austenitic steels represent a distinct category, combining the characteristics of both ferritic and austenitic steels due to their dual-phase microstructure. The presence of nickel influences the formation of the austenitic phase. These steels demonstrate superior

toughness, cold formability, weldability, and enhanced high-temperature strength compared to purely ferritic steels. Additionally, the onset of brittleness due to grain growth is delayed to higher temperatures. Furthermore, ferritic-austenitic steels exhibit improved resistance to sulphur-containing gases compared to conventional austenitic grades. (Li, Wenqiang et al., 2021)

Austenitic steels, characterized by their elevated nickel content, retain a stable austenitic microstructure, ensuring excellent thermal strength and toughness. These steels possess a significantly lower tendency to embrittle compared to ferritic steels. Brittleness, if it occurs, is typically observed only after prolonged exposure at specific temperature ranges and does not manifest above a certain threshold. Austenitic steels also demonstrate exceptional scaling resistance in oxidizing environments; however, they remain vulnerable to reducing agents in sulphurous gases. They offer excellent cold formability and can be welded using virtually all conventional welding techniques.

Superheater materials must withstand high operating temperatures, necessitating exceptional heat resistance and creep strength. These materials must also endure fire exposure and resist hot corrosion. The heat resistance of steels can be enhanced through alloying additions tailored to optimize specific properties. Low-alloy steels, including 10CrMo910, 13CrMo44, and 16Mo3, as well as high-alloy steels such as austenitic X6CrMo1713 and martensitic steels like X20CrMoV121 or X10CrMoVNb9-1, exhibit superior corrosion resistance, mechanical strength, and flaking resistance under high-temperature gas exposure. This study focuses on 16Mo3 steel, which was employed in a power plant application and serves as the primary subject of interest.

Chromium plays a key role in stainless steel alloys due to its ability to form a stable, protective oxide layer when exposed to oxygen, which significantly improves corrosion resistance. For a steel to be considered stainless, it must contain a minimum of 12% chromium. To maintain an austenitic crystal structure, elements such as nickel or manganese are typically added. Molybdenum is included to boost resistance to both general and pitting corrosion, while copper is beneficial in protecting the steel in acidic environments.

The determination of pipeline wall thickness follows pressure vessel standards, requiring calculations based on the selected materials and their associated mechanical properties. In addition to material expenses, installation labour costs must also be considered. Typically,

the most cost-effective material is selected from the available alternatives following comprehensive calculations. While low-alloy steels offer a more economical option, high-alloy steels may be preferable for applications involving high operating pressures due to their superior creep strength, which allows for the use of thinner-walled pipes while maintaining the required performance characteristics. Furthermore, highly alloyed steels exhibit reduced weight and lower material strength. However, low-alloy and carbon steels provide better thermal conductivity compared to their high-alloy counterparts. (Kalliokoski J, 2013; Li, Wenqiang et al., 2021.)

3.5 Welding of Steel

Welding involves fusing materials at elevated temperatures, either with or without additional filler metals. While steels are generally weldable, extreme thermal and chemical conditions necessitate specialized welding techniques.

The welding process is influenced by factors such as current, heat input, and penetration depth, all of which affect weld integrity. Strength calculations determine the required weld dimensions to ensure structural performance. (Souza & SpringerLink, 2012.)

In conclusion, the metallurgical principles governing steel phase transformations, alloying, heat treatments, and welding techniques enable the optimization of steel properties for diverse industrial applications, including structural engineering, tool manufacturing, and high-temperature environments.

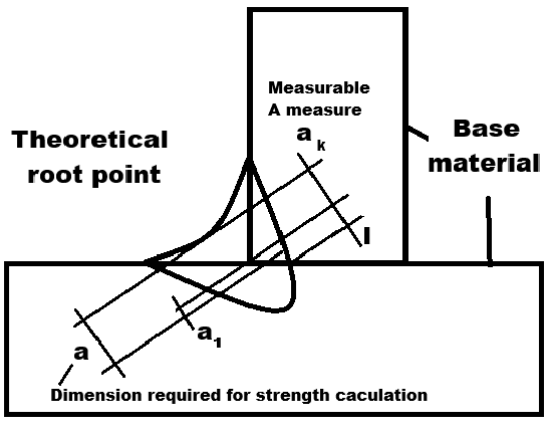

Figure 6. Weld A dimension

The welding process involves intense and rapid temperature changes that alter both the physical properties of the material and the internal stress distribution in the welded section. These thermal effects are concentrated in a specific region adjacent to the weld, referred to as the heat-affected zone (HAZ). The size and shape of the HAZ—its depth and breadth—are determined largely by the amount of heat introduced during welding. As a result, various microstructural regions develop around the weld, each exhibiting different material characteristics due to the localized heating and cooling cycles.

Thermal fluctuations and stress variations contribute to undesirable deformations in the welded assembly and result in heterogeneous microstructural formations within the HAZ and adjacent regions. Due to the localized melting of the material in the weld seam, macro-scale geometric discontinuities may arise, while microcracks can develop in its vicinity due to the rapid thermal cycling (Martikainen, 2015; Souza & SpringerLink, 2012).

Residual Stresses in Steel Structures - During processing and fabrication, steel structures may develop internal residual stresses, which are secondary in nature as they occur in the absence of external loads. These stresses typically originate from non-uniform cooling, localized heating—such as that caused by flame cutting or welding—or phase transformations at lower temperatures due to the decomposition of austenite. This phenomenon is particularly prevalent in the welding of high-strength steels, such as those used in structural components like the gripper under consideration. Additionally, cold forming can contribute to residual stress accumulation.

Defects in welded joints can arise from improper welding parameters, such as incorrect cooling time between passes, excessive heat input, or an insufficiently treated weld area. Residual stresses may persist within the material due to variations in crystal structure separation or the expansion of microstructural features formed during cooling.

Furthermore, the use of an incompatible filler material in combination with the base metal may lead to a weld joint of inferior quality. Such defects may be either visually observable or detectable using non-destructive testing (NDT) techniques, including dye penetrant inspection or ultrasonic testing, which can identify inconsistencies in the weld before the material undergoes failure.

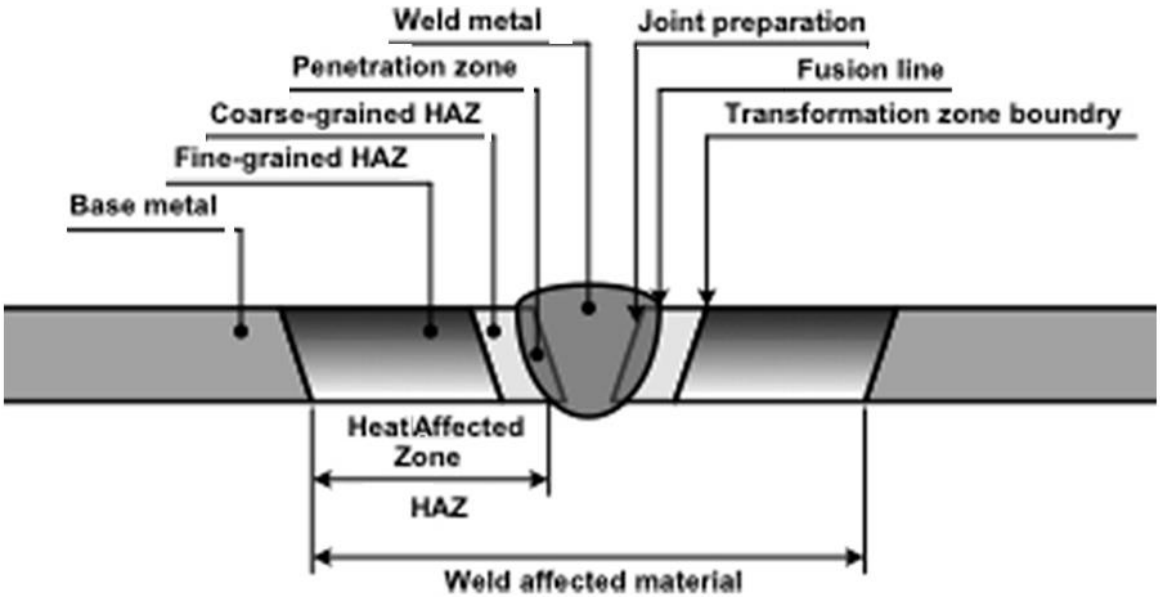

Figure 7. Different zones around the welding area

Microstructural Transformations During Welding - During the solidification phase of welding, the transformation of the structure from beta-ferrite to austenite is not permanent; instead, it begins to disperse as the temperature decreases below the A3 transformation temperature (723°C). The heat input during welding influences the microstructure of both the base material and the weld seam through thermal conduction.

As the welded joint cools, the microstructure of the weld seam undergoes a complete transformation into austenite once the temperature exceeds the A3 threshold. In the temperature range between A1 and A3, only partial austenitization occurs. Below the A1 temperature, a phenomenon known as high-temperature emission takes place, leading to the formation of small-angle grain boundaries. The region where these microstructural transformations occur is referred to as the transformation zone, commonly known as the heat-affected zone (HAZ) (Souza & SpringerLink, 2012).

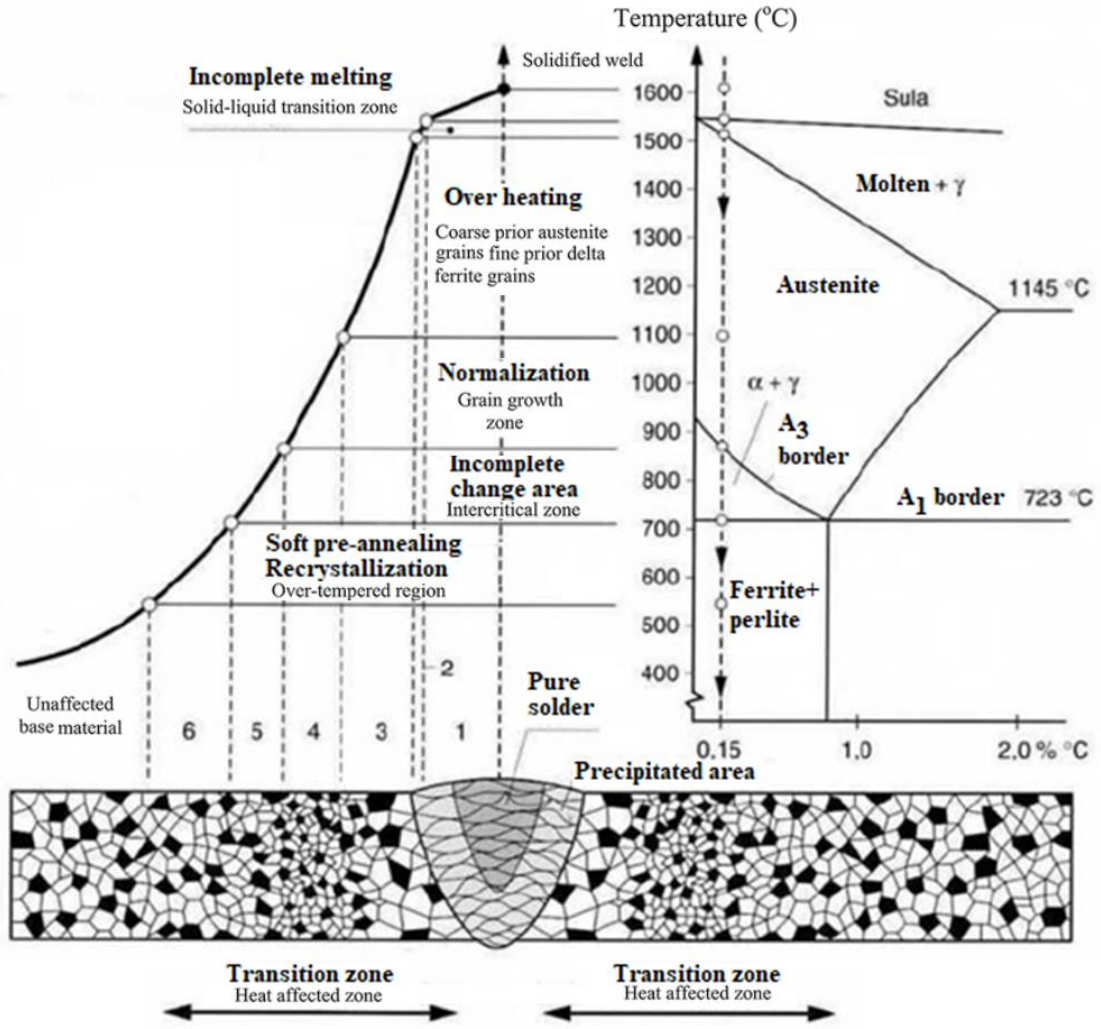

Figure 8. HAZ areas of unprecipitated carbon steel (Martikainen J. 2015).

1. Weld metal, which is a mixture of base material and welding additives.
2. Melt boundary area, where partially melted base material and weld material have mixed.
3. Coarse grain area (CGHAZ) (Coarse Grain, HAZ), where the temperature was 1100-1500°C. An austenitic transformation has occurred, and the austenite grain size has increased. Larger grain sizes than in the base material weaken impact resistance.
4. Fine-grained zone (FGHAZ) (Fine Grain, HAZ), where the temperature has been in the austenite zone, above the A3 temperature zone (850-1100°C).
5. Partially austenitized zone (ICHAZ) (Intercritical HAZ), where the temperature has been between the A1 and A3 temperatures (750-850°C).
6. Carbide spheroidization zone (SCHAZ) (Sub Critical HAZ), where the temperature is 600-750°C, corresponding to emission at high temperatures.

The most harmful of the transformation zones is the section with a rough structure, where the hardness and impact resistance are dependent on the cooling time. Hardness depends on the amount of martensite formed in the material. Hardness is most measured by an impact test, where the area of impact with the conical impact point is proportional to the obtained penetration in the material. In terms of hardness, the seam also has the potential for cold cracking (Martikainen J. 2015; Souza, Gilberto Francisco Martha de, and SpringerLink 2012).

The impact resistance is measured in the middle of the seam and at the edge of the welded melting point, approximately 1-2 mm. The most common way to influence the problems of the welding seam is preheating, in which case the thermal shock is smaller, and/or when the piece is welded, it is rejuvenated or softened, so to speak, minimizing the stresses in the area (Souza, Gilberto Francisco Martha de, and SpringerLink 2012).

3.6 Grain Size

Steel's mechanical performance is enhanced by reducing its grain size, which increases strength and toughness. To control grain refinement, adjustments are made to the material's composition, formation process, and heat treatment. Metallographic analysis using microscopy allows for the evaluation of a sample’s structural integrity by examining the size and uniformity of its grain distribution.

Grain structure research plays a critical role in ensuring safety and reliability across various industries. In aerospace, for instance, the grain characteristics of aluminium components in landing gear are closely monitored to prevent failure under stress. Similarly, the automotive industry relies on detailed grain analysis of steels and alloys to verify that critical parts can endure demanding operational conditions.

The grain size of the metal is a factor that affects the properties of the steel. The size of an individual grain when solidified can typically vary from 0.5 μm to several millimetres. A grain boundary forms between two grains, which is made visible after surface grinding and polishing by etching the metal surface with a suitable etching agent. This makes the grain boundaries, and the grains stand out to the human eye. The grain size itself affects the properties of the steel, such as strength and toughness.

The grain size can be determined using standards such as ISO 643 or ASTM E112. International standards for grain size analysis include ASTM E112 (USA), ISO 643 (Global), ASTM E1382 (USA), DIN 50601 (Germany), JIS G 0551 (Japan), JIS G 0552 (Japan), GOST 5639 (Russia), and GB/T 6394 (China).

The ASTM E112 standard test methods are the most common for determining grain size, as quality control laboratories use the ASTM diagram comparison method for grain analysis. In this method, a visual assessment of grain size is performed by comparing the model image in a microscope directly or in space. Based on that, the attributes given in the standard and the grain size are evaluated. However, due to the visual evaluation, the method may produce imprecise and unrepeatable results, which are generally not repeatable by different users. Additionally, the obtained results are recorded manually in the systems, which means that incorrect entries can weaken the credibility of the results. (Souza, Gilberto Francisco Martha de, and SpringerLink 2012)

As temperature rises, grain growth becomes more rapid, leading to an overall increase in grain size. This growth continues over time until it reaches a limit defined by the geometry of the component. Finer grains result in a greater total grain boundary area and higher bonding energy within the material. The majority of grain enlargement typically happens within the initial minutes of heating, after which the rate decreases and eventually stabilizes. Elevated temperatures encourage significant expansion of austenite grains. However, this can be controlled by incorporating specific alloying elements like aluminium and vanadium, which inhibit excessive grain growth. In practice, minimizing austenite grain size is preferred, as it promotes the formation of fine-grained ferrite, pearlite, or martensite, enhancing the steel's mechanical properties.

The reduction in grain size affects the properties of the steel, such as an increase in strength, especially in yield strength. Impact resistance improves and hardness increases because there are more bonds in the metal, making it "tougher and at the same time more brittle." An increase in grain size, however, improves the steel's elongation and shrinkage properties, as well as its formability.

Carbon is the most important alloying element in steel. With low carbon contents, iron is always in the form of ferrite, where it is soft, tough, and easily malleable. The formation of the microstructure of steel with different carbon contents and at different temperatures can

be deduced from the iron-carbon phase diagram shown in Figures 8 and 12. When the carbon content in the steel exceeds 0.05%, pearlite starts to appear alongside ferrite. Pearlite is a mixture of ferrite and cementite. Pearlite is not as malleable as ferrite but has good tensile strength. (Souza, Gilberto Francisco Martha de, and SpringerLink 2012.)

When pure iron is heated to a high temperature, after more than 911ºC, its crystal form starts to change to austenite. In this case, austenite is able to dissolve a significant amount of carbon, unlike the ferritic form. The austenite begins to disperse again as the temperature decreases below the A3 temperature and disperses completely when the temperature drops below the A1 range. This creates a ferritic-pearlitic microstructure with carbon contents below 0.8%, where the proportion of pearlite increases as the carbon content increases. At a carbon content of 0.8%, the microstructure is completely pearlitic, and at concentrations above 0.8%, cementite also occurs as grain boundary cementite at the grain boundaries of the pearlitic base material. Grain boundary cementite is hard and very brittle.

A martensitic microstructure, or hardened structure, is achieved by rapidly cooling the steel from a temperature above 750ºC. Martensitic steel is hard, and its hardness improves even more as the carbon content increases. Hardened steel often contains chromium, nickel, tungsten, molybdenum, or vanadium, which improve the hardenability of the steel. (Souza, Gilberto Francisco Martha de, and SpringerLink 2012, Mohammadi Zahrani, E., and A.M. Alfantazi, 2021.)

3.7 High-strength steels

Hot-strength steels have good and well-defined strength properties at high operating temperatures, up to approximately 650 ºC, depending on the steel type. Typical applications include the steam cylinder of a steam boiler plant, evaporators, steam pipelines, manifolds, heat exchangers, finned tube panels, and heaters. Additionally, these steels are used in applications in the chemical and petrochemical industries, as well as in hydrogen reactors in energy production plants.

At high operating temperatures, steels must exhibit excellent creep and fatigue resistance. This is achieved through alloying and treating the steel to develop the desired properties.

Processing methods include steel hardening, rejuvenating, cold or hot rolling, and annealing, which is also called tempering.

When steel is hardened, it is heated to a red-hot temperature of more than 911 ºC, and then rapidly cooled in water, for example. Afterward, the steel is tempered, meaning it is lightly annealed. Annealing refers to heating the steel to a red glow to remove or reduce residual stresses or similar unwanted properties of the piece. This process makes the steel harder and more durable. Rejuvenation is similar to hardening, but in this case, the steel is brought to a slightly higher temperature than in hardening. This results in steel that is strong and tough, but with decreased hardness. Rolling, on the other hand, involves shaping steel with rollers, either through cold or hot rolling. (Li, Wenqiang et al., 2021.)

Strength properties in hot temperatures is improved with alloys, with molybdenum being the most common and effective, despite its high material cost, as only a small amount is required. Together with iron, molybdenum forms heat-strengthening crystals that differ in size from others, improving the bond energy between the bonds. Other common alloying elements include chromium, niobium, vanadium, nitrogen, and aluminium. The primary function of chromium is to enhance resistance to corrosion and oxidation. Chromium content for higher temperatures can be as high as 12%. Niobium, vanadium, and nitrogen form strengthening carbides and nitrides, which bond the alloy. Heat resistance can also be increased by reducing the amount of carbon, as its reinforcing effect weakens and eventually becomes detrimental at higher temperatures.

The demand for more stress-resistant steels has led to changes in the shape of many basic metals. Through years of experience, these materials have developed significantly, resulting in thinner and lighter materials with improved properties, allowing for the achievement of the required properties using less material. (Sikanen, T. 2019; Kauppi T. 2013.)

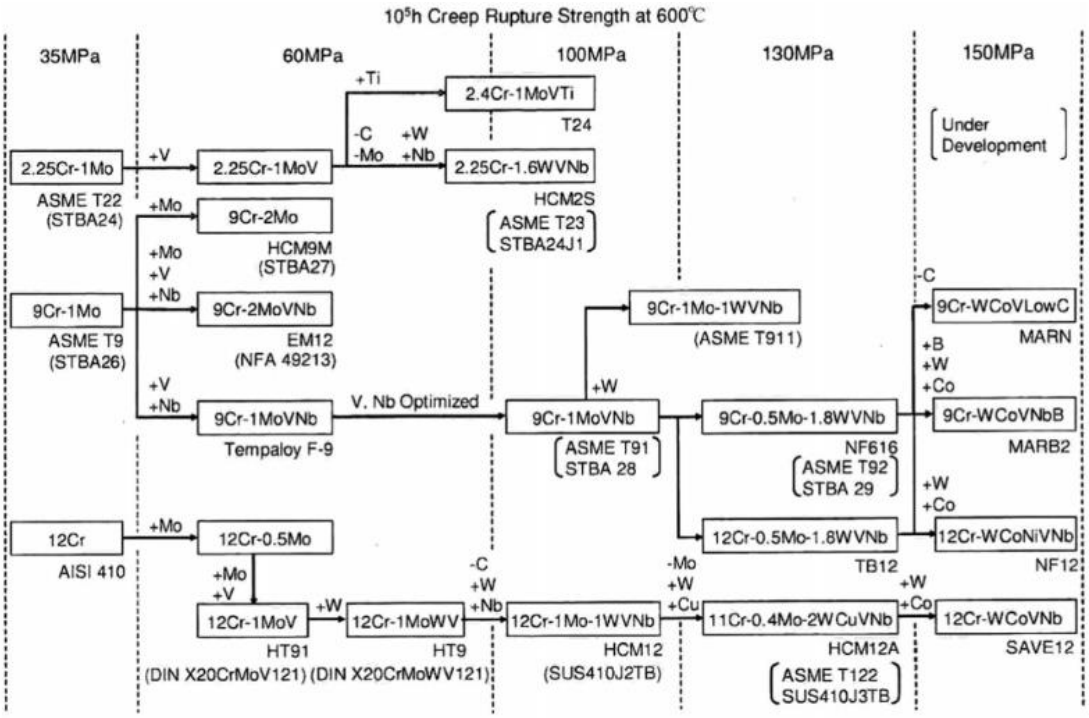

Figure 9. Example of progressive development of 9–12%Cr steels 64,67 (Kalliokoski, 2013).

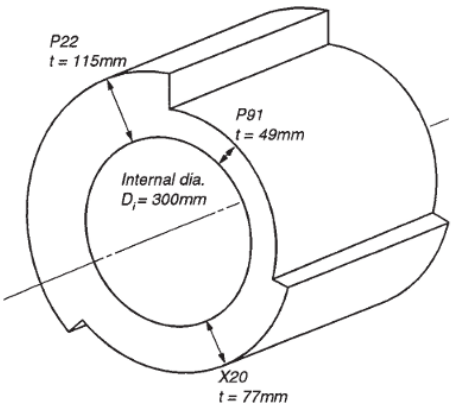

Figure 10. Comparison example on wall thickness achievable through use of advanced 9%Cr parent alloys: temperature 5600uC; pressure 530 N mm22; 100 000 h life94 (Kalliokoski, 2013).

3.8 Studying the microstructure of metal

The copy-checking method is a non-destructive testing (NDT) technique used to examine metal microstructures under operational conditions. It involves pressing a softened plastic film onto a polished and etched metal surface to replicate its microstructure. After hardening, the impression can be analysed using light or electron microscopy. This method offers high resolution (<0.1 µm), enabling early detection of creep damage.

The impression is taken from the most damaged region of the component to assess microcracks and cavity density, aiding in creep classification and lifetime evaluation. Coating the replica enhances its clarity and evaluation accuracy.

While visual inspection provides basic information on fracture type and failure mechanisms, it does not offer detailed insights into the internal structure. However, it remains useful when supplemented with microscopic analysis (Kalliokoski, 2013).

3.9 Weldability of High-Strength Steels

The coarsening tendency is a factor to consider in steel, particularly in relation to the cold cracking tendency, i.e., the hydrogen cracking tendency. Generally, as the alloying content increases, the weldability of the steel decreases. The carbon equivalent is used to express the effect of the concentration of different alloying substances contained in the alloy on weldability (proneness to hydrogen cracking).

The higher the carbon equivalent, the rougher the steel, requiring more preheating and post-heating treatment. The most well-known carbon equivalent formula (in table 1) is the so-called IIW formula:

$$Ce\ (IIW) = C + Mn/6 + (Cr + Mo + V)/5 + (Ni + Cu)/15 \quad (1)$$

, which allows the calculation of the weldability value (Kalliokoski J 2013).

Table 1. Carbon equivalent CE values for heat-resistant steels

Steel	C%	Mn%	Cr%	Mo%	V%	Ni%	Cu%	CE
S355GH	0.10	1.10						0.28
	0.22	1.70	0.30	0.08	0.02	0.30	0.3	0.62
16Mo3	0.12	0.40	0.30	0.25	0.00	0.00	0.3	0.32
	0.20	0.90	0.30	0.35	0.00	0.00	0.3	0.50
10CrMo9-10	0.08	0.40	2.00	0.90				0.73
	0.14	0.80	2.50	1.10				1.01

Based on the calculated (IIW) values, well-weldable steels include P235GH and 16Mo3, while limited-weldable steels are 15NiCuMoNb5-6-4 and 10CrMo9-10. In addition, very limited-weldable steels are high-alloy steels for which the carbon equivalent formula is no longer applicable, such as 10-12CrMo, X10CrMoVNb9-1, and X20CrMoV11-1 steels, with "X10" being clearly better than "X20." Most alloyed steels are so hardened that they require preheating before welding, which must also be considered during the welding of intermediate pieces. At the end of the annealing process, the seam and its nearby HAZ area undergo a controlled post-heat treatment to normalize the crystal structure and stresses, minimizing the possibility of failure.

Welding Preheating - Preheating before welding and post-welding heat treatment are crucial to ensuring welding quality. All-important pressure equipment welding requires preheating before welding. The main tasks of preheating include influencing factors such as slowing down the cooling rate of the created weld seam, thus facilitating the exit of diffused hydrogen from the weld metal and preventing hydrogen-induced cracks. At the same time, preheating reduces the hardness of the weld and improves the crack resistance of the joint and the properties of the HAZ area. In addition, preheating reduces welding stress by minimizing the temperature differences between materials after thermal expansion is reduced, which in turn helps prevent cracking of the seam area.

The selection of the preheating temperature and the temperature of the intermediate layer is influenced by the welding method, ambient temperature, and the chemical composition of the material. The uniformity of the preheating temperature in the thickness direction of the steel sheet and in the welding, area significantly affects the reduction of welding stress. As a rule of thumb, the width of the preheating area is usually three times the wall thickness

around the welding area (Li, Wenqiang et al. 2021; Mohammadi Zahrani, E, and A.M. Alfantazi. 2021).

Post-Welding Heat Treatment - The main purposes of post-welding heat treatment are to remove post-weld hydrogen from the seam, eliminate welding stress, and improve the weld structure and performance. Post-welding dehydrogenation heat treatment takes place after welding, when the weld has not yet cooled below 100°C. Generally, the seam area is heated to 200–350°C for 2-6 hours. This process helps to accelerate the removal of hydrogen from the weld seam and reduces the effect of welding heat from surrounding areas, thus effectively preventing cracks in the welding of low-alloy steel.

Due to the uneven heat distribution during welding and subsequent cooling, welding stresses almost always arise after the welding work is finished. These stresses reduce the actual durability of the welded joint area and may cause plastic deformation or even material breakage.

Stress-reducing heat treatment prevents the reduction of yield strength at high temperatures. One method for this is high-temperature hardening, where the entire weld seam is placed in a heating oven, or the material is heated in place to a desired temperature, where it is held for the required time and then cooled in air or with a controlled decrease in temperature to normal levels. During annealing, the steel is heated to 550–750°C for 1–2 hours to remove or significantly reduce internal stresses in the material.

In this way, 80%-90% of the welding stress can be eliminated. The second method is a similar local high-temperature hardening approach, where only the weld and its surrounding area are heated and then cooled slowly, resulting in partial removal of the welding stress. After heat treatment, the plasticity and toughness of the welded joint improve, and the metallographic structure and mechanical properties are enhanced (Li, Wenqiang et al. 2021; Mohammadi Zahrani, E, and A.M. Alfantazi. 2021).

3.10 Failure mechanisms in power plant boilers

Common Failure Mechanisms in Power Plant Boilers - Power plant boilers are subject to a range of degradation mechanisms that can compromise structural integrity and operational reliability. The predominant failure modes include erosion, corrosion, creep, fatigue,

cracking, and the accumulation of internal deposits on boiler tubes. Detecting these faults often requires specialized diagnostic tools, such as thermal imaging systems or non-destructive testing (NDT) techniques, due to the inaccessibility of internal surfaces.

Corrosion Mechanisms - Corrosion is defined as the material degradation, particularly of metals, due to chemical or electrochemical interaction with the surrounding environment. This phenomenon typically results in the loss of material and the initiation of surface or subsurface defects. In their natural state, metals are usually present as thermodynamically stable compounds—such as oxides, silicates, or carbonates. Once refined, metals become energetically unstable and tend to revert to these stable forms when exposed to environmental conditions, leading to corrosion.

The degradation can proceed via direct chemical reactions with aggressive species or through electrochemical pathways involving anodic and cathodic regions on the metal surface. In electrochemical corrosion, anodic areas undergo material loss in the form of ions, while electrons flow to cathodic sites, completing the circuit.

Corrosion in Waste Incineration Boilers - In waste-to-energy plants, corrosive degradation is often intensified due to the chemical composition of the flue gases generated during combustion. These gases typically contain sulphur compounds, oxygen, and chlorine species, which can condense or react on heat-exchange surfaces. The result is the formation of complex deposit layers composed of oxides, salts, and molten slag. Such deposits promote severe forms of corrosion, including hot corrosion, where high-temperature reactions involving sulphur trioxide (SO_3) and chlorinated compounds are prevalent.

High-Temperature and Localized Corrosion - Corrosion rates generally increase with temperature, particularly under oxidizing furnace conditions. This effect, referred to as high-temperature scaling, involves the accelerated formation and spallation of oxide layers at elevated temperatures.

Localized corrosion, such as pitting, occurs when aggressive ions (notably chloride ions, Cl^-) concentrate in confined areas. These localized environments can create electrochemical cells with micro-anodic sites, leading to rapid penetration and damage. Factors contributing to such conditions include surface roughness, flow-induced turbulence, and the presence of crevices.

In heat exchange components like economizers and air preheaters, operating temperatures can drop below the acid dew point (approximately 150 °C), causing acidic vapours to condense. The resulting acidic condensates, particularly sulfuric or hydrochloric acid, are highly corrosive and further exacerbate material degradation.

Stress Corrosion Cracking and Hydrogen Embrittlement - When materials are exposed to both tensile stress and a corrosive setting, they can experience stress corrosion cracking (SCC), a failure mechanism where cracks develop and grow over time. This phenomenon is especially common in austenitic stainless steels, which are vulnerable in hydrogen-rich environments. In such cases, hydrogen can infiltrate the metal's structure, leading to hydrogen embrittlement. This condition is particularly problematic in high-strength alloy steels, as it significantly diminishes their ductility and resistance to fracture. (Arora, P., Singh, P.K., Bhasin, V., Vaze, K.K., Ghosh, A.K., Pukazhendi, D.M., Gandhi, P., & Raghava, G. 2011)

Figure 11. Example of corrosion (Lathrop Trotter's blog post, 2020; XMPro's official website, 2020).

Hot Corrosion - The reaction temperature has a positive effect on the rate of hot corrosion progression. Sulphur, sodium, and vanadium, which are carried with the fuel, usually cause hot corrosion. Hot corrosion is problematic because it causes pitting, especially in iron-, nickel-, and cobalt-dominated high-temperature alloys, at a high rate. The fly ash in the flue gases contains partly melted ash, which easily sticks to the heat transfer surfaces. This can sometimes quickly lead to the disintegration of the oxide layer under the ash and severe corrosion of the metal surface.

Hot corrosion depends on the fuel, which contains heavy metals, chlorides, and other substances that melt at a low temperature. When using chlorine-rich fuel, chlorine corrosion can occur, and the damage caused by this may only be visible after weeks or even months. Ferric chloride forms on the surface of the steel, and when vaporized, it reacts with oxygen to form iron oxide and gaseous chlorine. The gaseous chlorine then reacts with another steel surface to form ferric chloride, and the cycle starts again, even if no new chlorine is introduced with the fuel.

Creep - a time-dependent deformation behaviour which occurs in materials that are exposed on high temperatures and sustained loads below their yield or elongation limits. Over prolonged periods, this can result in irreversible strain, particularly under tensile stress. Assessing a material's creep resistance is essential in the structural design of components subjected to elevated temperatures.

Creep behaviour typically follows three stages. In the initial phase, the deformation rate slows progressively—a transient period. The second stage is characterized by a relatively constant deformation rate, marking a steady-state condition. In the final phase, the deformation rate accelerates, ultimately resulting in material failure.

The evolution of creep damage can be analysed through microstructural inspection. Early stages often reveal minimal changes, possibly just isolated voids at grain boundaries. As creep progresses, these voids may align or grow into microcracks. In the final phase, microcracks coalesce into larger cracks, eventually causing rupture.

When designing critical boiler components, it is vital to account for creep behaviour. The estimated operational lifespan of such parts is based on the expected creep rate and routine inspections. Early detection of creep-related degradation is crucial, which is why monitoring should commence once around 80% of the component's anticipated life has elapsed, or earlier if signs of damage appear.

Creep failures commonly develop in the heat-affected zones of welded joints, rather than in the base metal itself, as these transition areas are more susceptible to thermal and mechanical stress. In high-pressure steam lines, creep is often the primary factor limiting service life. Notably, severe creep failures have been observed even in systems designed for extended operation, often due to inadequate mechanical support or stress concentrations in welded zones. (Arora, P., Singh, P.K., Bhasin, V., Vaze, K.K., Ghosh, A.K., Pukazhendi, D.M.,

Gandhi, P., & Raghava, G. 2011; Khedr, M., Abd Elaziem, W., Newishy, M., & Abdel-Aleem, H. 2023; Li, Wenqiang et al. 2021.)

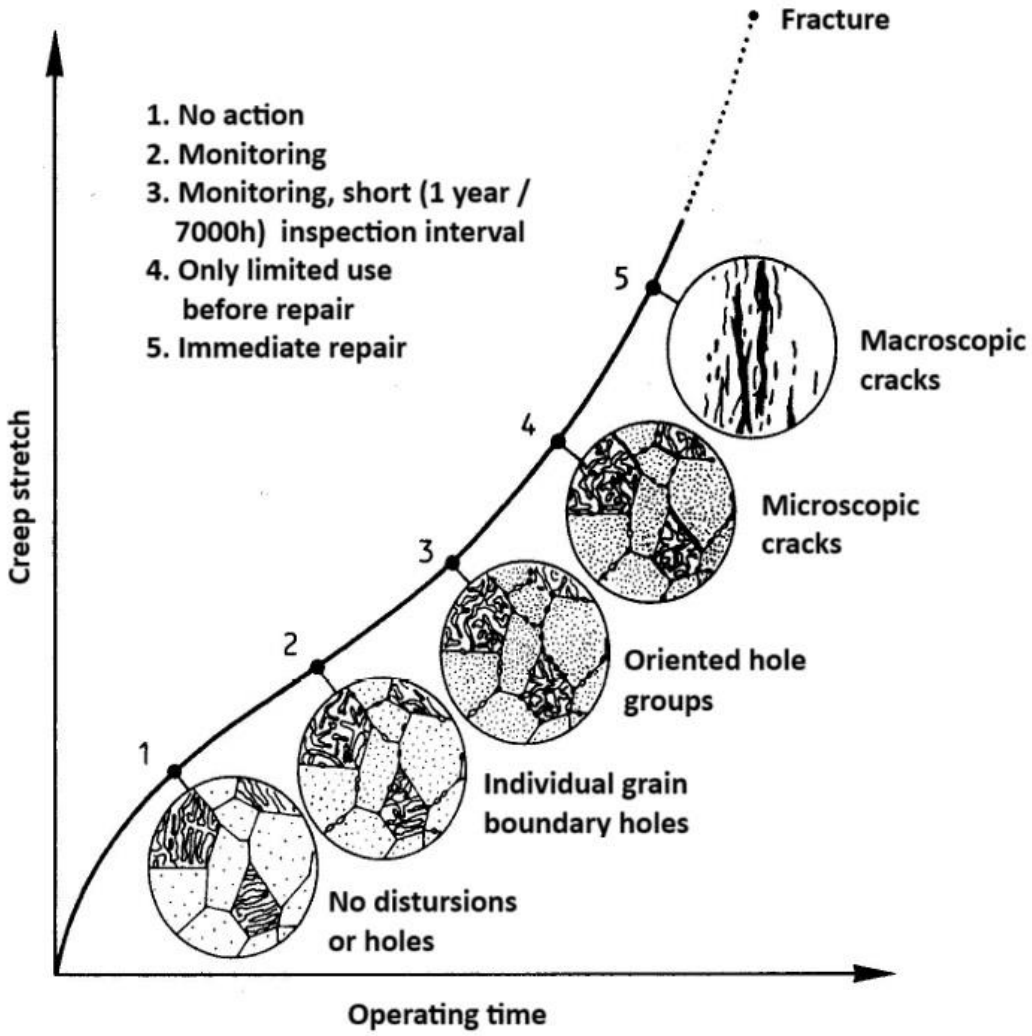

Figure 12. Example of creep crack development before repair

Fatigue - The fatigue process is a dynamic, cyclical stress on the material. In static, uniform loading, the reference stress reaches the breakage point of the material, causing the object to brake. In dynamic loading, the fracture process is more complicated because the load constantly changes, and the material experiences several microscopic damages. These damages accumulate and, together, cause the piece to brake. The fatigue process involves the creation of visible initial distortion and the progression of that distortion. Fatigue is a complex process affected by many laws of material theory, as well as aspects of elasticity

and plasticity theory. In power plant boilers, parts under changing loads are particularly vulnerable to fatigue.

Erosion - Erosion is pure mechanical wear of the material caused by flue gases and their particles in steam boilers. Erosion affects the cooking surfaces of the boiler and other steel structures. In addition to the mass and hardness of the particles, the impact speed and the angle at which the particles hit the material also influence the erosion. Erosion is also caused in recirculating boilers by sand circulating in the hearth along with the airflow.

Erosion affects all parts of the firebox, such as vaporizer pipes, masonry, and cyclones through which sand passes during the combustion process. Flue gases and fly ash cause erosion primarily in heaters and economizers. As a result of erosion, the pipe thickness decreases over time.

Furthermore, steam scrapers can cause erosion, even though they are an essential part of steam boiler cleaning and improve the thermal conductivity of cooking surfaces by removing impurities. Erosion can be reduced by selecting different materials or protecting objects with, for example, protective gutters or wear plates.

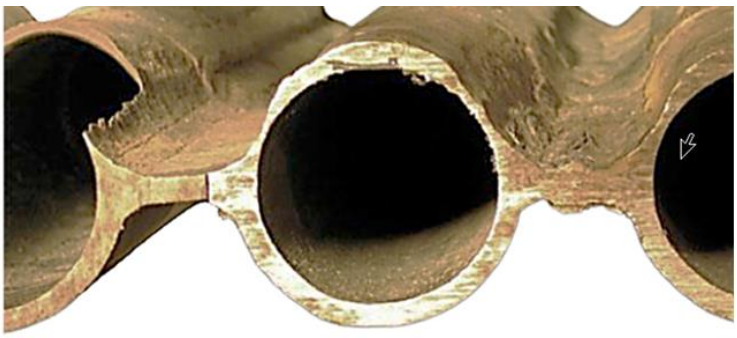

Figure 13. Example of abrasive erosion of boiler cooking pipe frame wall

Sulphur - Sulphur began to be fed into boilers after the burning of sulphurous peat decreased, in order to prevent chlorine corrosion. Sulphur itself does not cause harm in the combustion process at such high temperatures. However, sulfur trioxide can still be generated thermally at temperatures above 1100°C and catalytically at lower temperatures around 500–800°C. The deposits formed on various surfaces of the boiler often act as catalysts. Sulphur compounds cause problems in the rest of the boiler, where the temperature drops below

140°C, such as in electric filters and flue gas ducts, particularly in ducts with leaks, which create local cooler spots that drop the temperature below 140°C.

Despite the small amount of sulfur trioxide, it can still cause corrosion depending on the temperature and moisture conditions. At low temperatures, sulfur trioxide combines with water to form sulfuric acid (H_2SO_4), which starts to condense as soon as the dew point of sulfur is lowered, easily causing corrosion of metallic surfaces.

Ammonia - Nitrogen oxides are removed by spraying ammonia, for example, directly onto the hot top section of the boiler (not a catalytic method) from different heights. There can be several spray points, which can be changed to achieve the desired result.

Ammonia can also be injected into flue gases using a catalytic method to bind nitrogen and achieve the desired NOx (oxides of nitrogen) values.

Welding Seam and Welding Area Defects - Weld defects are imperfections that arise when the welding process deviates from the intended procedures or parameters, leading to discrepancies in the weld's shape, dimensions, or overall quality. These flaws can appear either within the weld itself or in the surrounding material. Critical defects—such as cracking—are generally unacceptable due to their impact on structural integrity. However, some minor imperfections may be tolerated, provided they fall within the allowable limits specified by relevant standards or inspection criteria. (Ghosh, D., Ray, S., Mandal, J., Mandal, N. & Shukla, A.K. 2018; Arora, P., Singh, P.K., Bhasin, V., Vaze, K.K., Ghosh, A.K., Pukazhendi, D.M., Gandhi, P. & Raghava, G. 2011; Khedr, M., Abd Elaziem, W., Newishy, M. & Abdel-Aleem, H. 2023; Li, Wenqiang et al.2021.)

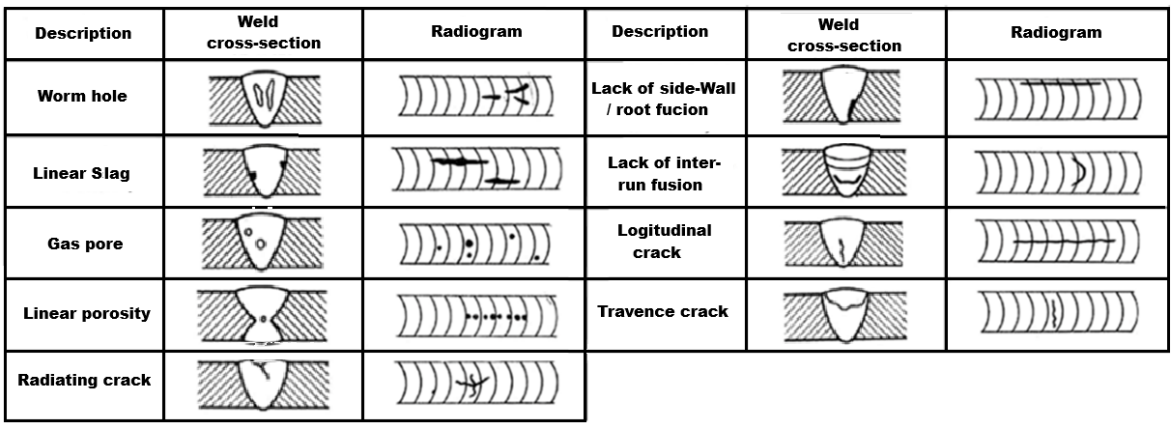

Figure 14. Different welding defects

High-strength steels undergo progressive microstructural changes when subjected to elevated temperatures and sustained mechanical loading. This phenomenon, often termed thermal-mechanical stress, alters the internal structure of the material and influences its mechanical performance, especially its load-bearing capacity at high temperatures.

These microstructural transformations—such as grain growth, phase decomposition, and carbide coarsening—can degrade the steel's mechanical properties over time, including tensile strength and hardness. To characterize and quantify these changes, a range of metallurgical analysis techniques are utilized. Common methods include optical microscopy for general microstructure observation, scanning electron microscopy (SEM) for high-resolution surface and phase analysis, and hardness testing to assess mechanical degradation and strength retention.

Understanding these microstructural developments is essential for predicting component lifespan and ensuring reliability in high-temperature service environments. The transformation of microstructure in ferritic-pearlitic steels occurs progressively through distinct stages. Initially, ferrite and pearlite phases are clearly distinguishable under microscopic observation. Over time, pearlite begins to lose its lamellar structure and transforms into a more spheroidal form, though remnants of the original structure may still be detected. As spheroidization advances, carbides continue to separate and spread throughout the matrix. Eventually, the microstructure becomes fully homogenized, with the original pearlitic regions disappearing and many carbides growing significantly in size. This progression directly influences the steel's mechanical properties and performance under stress. (Ghosh, D., Ray, S., Mandal, J., Mandal, N., & Shukla, A.K. 2018; Arora, P., Singh, P.K., Bhasin, V., Vaze, K.K., Ghosh, A.K., Pukazhendi, D.M., Gandhi, P., & Raghava, G. 2011; Khedr, M., Abd Elaziem, W., Newishy, M., & Abdel-Aleem, H. 2023; Li, Wenqiang et al. 2021.)

3.11 Properties of 16Mo3, EN 1.5415, DIN 15Mo3 Steel Used in the Boiler

16Mo3 steel belongs to a special steel group for pressure vessels, such as pipes in DIN 17155-1983, within the European standard code system. The steel is classified as low-alloy heat-strength steel, with the addition of 0.25 – 0.35 weight percent molybdenum to improve heat strength properties. It is a traditional "old school" steam boiler and pressure equipment

steel and belongs to material group SFS-EN 288-3 / CEN/TR ISO 15608. The highest operating temperature of this steel is usually 500°C, but it can still be higher. (Mohammadi Zahrani, E., and A.M. Alfantazi. 2021)

Table 3. Composition standard of 16Mo3 in weight presents (Kulawinski, Dirk 2019).

C	Si	Mn	Ni	P	S	Cr	Mo	N	Cu
0.12–0.2	**max 0.35**	**0.4–0.9**	**max 0.3**	**max 0.025**	**max 0.01**	**max 0.3**	**0.25–0.35**	**max 0.012**	**max 0.3**

Table 4. Mechanical properties (Kulawinski, Dirk et al. 2019).

Nominal thickness (mm):		to 250				**250–500**	
Rm - Tensile strength (MPa) (+QT)		**440–570**				**420–550**	
Nominal thickness (mm):		to 60			**60–100**	**100–150**	**150–250**
Rm - Tensile strength (MPa) (+N)		440–590			**430–580**	**420–570**	**410–570**
Nominal thickness (mm):		**to 16**	**16–40**	**40–60**	**60–100**	**100–150**	**150–250**
ReH - Minimum yield strength (MPa) (+N)		**275**	**270**	**260**	**240**	**220**	**210**
Nominal thickness (mm):		**to 250**			**250–500**		
ReH - Minimum yield strength (MPa) (+QT)		**265**			**250**		
A - Min. elongation at fracture (%) longitud., (+QT)		**23**					
A - Min. elongation at fracture (%) transverse, (+N)		**20**					
Nominal thickness (mm):		**to 40**		**40–60**	**60–100**	**100–150**	
A - Min. elongation at fracture (%) (+N)		**24**		**23**	**22**	**19**	

Table 5. Equivalent grades (Kulawinski, Dirk et al. 2019).

EU EN	USA -	Germany DIN, WNr	Japan JIS	France AFNOR	England BS	Italy UNI
16Mo3	A204Gr.A A204Gr.B	15Mo3 16Mo3	STBA12	15D3	1503-243B 240 243	15Mo3 16Mo3
Spain UNE	Sweden SS	Poland PN	Czechia CSN	Austria ONORM	Inter ISO	Best as known
16Mo3	2912	16M	15020	15Mo3KW	F26 P26 TS26	15Mo3 16Mo3

Standards (Mohammadi Zahrani, E., and A.M. Alfantazi. 2021; Kulawinski, Dirk et al. 2019):

EN 10028-2: 2009 - Flat products made of steels for pressure purposes. Non-alloy and alloy steels with specified elevated temperature properties.

EN 10222-2: 2000 - Steel forgings for pressure purposes. Ferritic and martensitic steels with specified elevated temperature properties.

EN 10216-2: 2014 - Seamless steel tubes for pressure purposes. Technical delivery conditions. Non-alloy and alloy steel tubes with specified elevated temperature properties.

EN 10217-5: 2002 - Welded steel tubes for pressure purposes. Submerged arc welded non-alloy and alloy steel tubes with specified elevated temperature properties.

EN 10217-2: 2002 - Welded steel tubes for pressure purposes. Electric welded non-alloy and alloy steel tubes with specified elevated temperature properties.

EN 10253-2: 2007 - Butt-welding pipe fittings. Non-alloy and ferritic alloy steels with specific inspection requirements.

EN 10273: 2007 - Hot rolled weldable steel bars for pressure purposes with specified elevated temperature properties

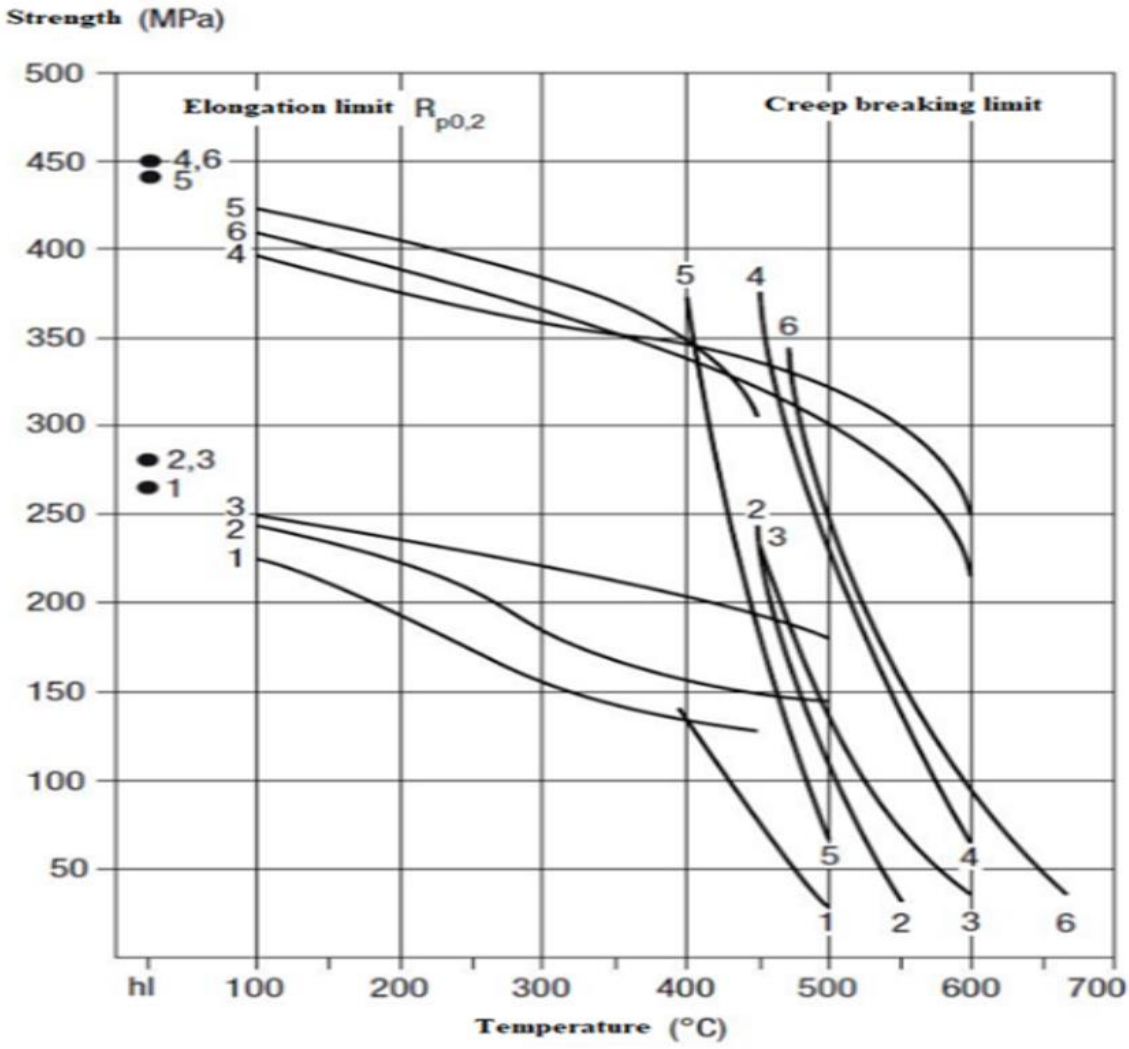

Figure 15. 0.2% elongation limit and 100,000-hour creep rupture limit of high-strength steels (SFS-EN 10216-2). Steels: 1: P265GH, 2: 16Mo3, 3: 10CrMo9-10, 4: 7CrMoVTiB10-10 (T/P24), 5: 15NiCuMoNb5-6-4´ (WB 36) and 6: X10CrMoVNb9-1 (T/P91). (Tanja Winqvist, Johanna Tuiremo, 2017.)

3.12 Theoretical Possibilities

Grain Growth and Its Role in Polycrystalline Materials - Grain growth is a fundamental process that plays a vital role in shaping the physical and mechanical characteristics of polycrystalline materials. It has been the focus of extensive investigation through both theoretical modelling and laboratory experiments over many decades.

In their study titled "Grain Growth in Anisotropic Systems: Comparison of Effects of Energy and Mobility," A. Kazaryan, Y. Wang, S.A. Dregia, and B.R. Patton explore how variations in grain boundary energy and mobility—both of which can be directionally dependent—affect the evolution of grain structures. Their work utilizes computational simulations to model a two-dimensional textured polycrystalline material, allowing for both grain boundary misorientation and inclination to influence energy and mobility.

The authors use a phase field modelling approach to assess the individual and combined effects of energy and mobility anisotropy. Their findings show that anisotropic energy leads to significant deviations from typical isotropic growth behaviour. This results in uneven grain boundary distributions and misorientation patterns that favour the development of low energy, elongated, and sharply defined grain structures.

Further simulations using generalized phase field models that incorporate orientation-dependent boundary mobility confirm that although mobility anisotropy influences the rate of growth over time, the overall statistical features of grain orientation and size remain relatively consistent—whether energy and mobility anisotropies act independently or together.

It is widely recognized that both grain boundary energy and mobility vary with boundary orientation and angle, making them inherently anisotropic. Interestingly, the influence of mobility anisotropy on growth dynamics becomes significant only in the presence of energy anisotropy. Time-dependent changes in the distribution of grain orientations are a key factor in determining how grain structures evolve under these conditions.

Research combining simulations and experimental data consistently shows that while energy anisotropy affects growth behaviour, variations in mobility—often spanning several orders of magnitude—have an even greater influence on the kinetics of grain growth and the evolution of microstructures. Despite variations in individual grain behaviour, the overall statistical trends in grain size and distribution in anisotropic systems remain comparable to those observed under isotropic conditions, with only minor deviations in average grain area and orientation. (Moravec, Jaromir et al. 2019; Kazaryan, A et al. 2002; Kurek, Andrzej. 2020; Kulawinski, Dirk et al. 2019; Izaki, Toru et al. 2009.)

3.13 Design Curves in a Boiler

The design of boilers is best based on the knowledge of the stress that generates a certain total yielding in the metal over a specific time and temperature. For example, when dimensioning the tubes of a heater, the designer can best make use of information about what stress causes, for example, a total yield of 1% in 10,000 hours or a total yield of 5% in 100,000 hours. (Moravec, Jaromir et al. 2019.)

4 Simulation in welding processes

Today, simulating and modeling the welding process has become a very important and powerful tool due to the growing need in industrial applications and the design of ways to make welds reliable and low-cost. This allows users to predict how the welding process affects the material and change the elements that impact the weld without actual welding. After examining the results, the user can adjust the known starting values to the desired geometry and refine the simulation to predict if the same or better results can be achieved. Simulation can consider the different geometry of the weld piece, the mechanical behavior of the structure, and even predict the microstructure.

Simulation can be used to simplify the actual processes and provide an easy way to save materials and improve geometry. The only downside of welding simulation is that it requires much more data that can be measured to ensure the calculation takes into account the most essential aspects of the simulation. Additionally, the long calculation times demand significant computational power.

This is one reason why aspects are often simplified, and assumptions are made in the simulation as much as possible without compromising the result. Therefore, it is important to think ahead and set the parameters correctly to achieve both goals: accuracy and minimum calculation time, if possible. Even the simplest tasks or functions can be challenging to convert into numeric form so that calculations within the simulation are possible.

From the simulation, essential details can be effectively determined, such as the required welding method, welding speed, heat input, current used, heat distribution through the piece, welding tip angularity, and even ways to control the stem formation.

By using this information, many critical errors can be prevented before the actual process begins. The user can also simulate the path of the finished product to the customer. The main benefit is that many potential issues can be avoided if the simulation can predict where the error points are. Additionally, non-linear conditions can be taken into account while simultaneously optimizing the process. This is why it is necessary to have actual and realistic data foundations included in the simulation to achieve the best results (Silva, Lucas Filipe Martins da, Reza Beygi, and Eduardo Cesar Marques. 2022; Barzin, Behzad 2015; Richard

Rennie, and Jonathan Law. 2020; Afonine, Pavel V et al. 2015; Liu, G. R, H Nguyen-Xuan, and T Nguyen-Thoi 2010; Akin, J. E. 2005; Reda, Reham, Mohamed Magdy, and Mohamed Rady. 2020; Hyde, T.H et al. 2006).

5 Metallurgical simulation

For the base values, the average composition of 16Mo3 in volume percent was taken as the input composition for the MatCalc simulation. The composition used was as follows: C 0.15 w%, Cr 0.15 w%, Cu 0.15 w%, Mn 0.65 w%, Mo 0.3 w%, N 0.006 w%, Ni 0.15 w%, P 0.125 w%, S 0.005 w%, and Si 0.175 w%. The temperature range for the simulation and the reference point was set from 20°C to 1600°C in 25°C increments, as it occurs in the SAW and MIG welding processes. The SAW method was chosen for the simulation due to its lower heat input in the welding temperature range.

Phase composition was then simulated using the MatCalc simulation program as a function of temperature in figure 17, and the structural content in each temperature range was observed and analyzed for the simulation.

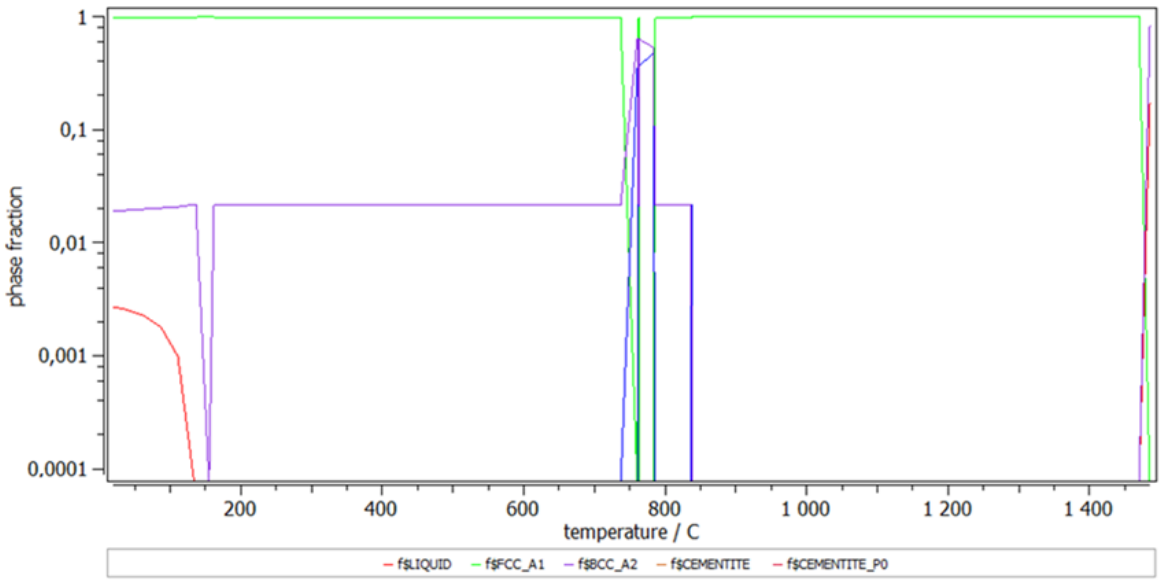

Figure 16. Phase composition in function of temperature and structural content

Also, the numerical structural content can be observed in connection with phase changes, as the structural composition varies with temperature. This provides a perspective on the composition and structure of each phase.

Structural steel is the most studied and therefore the best understood material. Its behavior under different conditions is predictable, and it is therefore subject to various standards and methods, such as the general Eurocodes, which define the cross-section, shape, chemical composition, and other mechanical properties. Still, most of its properties change significantly, especially during the welding process of high-strength steels.

In welding, localized regions of the workpiece are heated to their melting temperatures by a concentrated heat source, typically an electric arc. This applied thermal energy, known as heat input, is measured as the energy delivered per unit length of the weld. The extent to which the base material's properties are altered depends largely on the cooling rate within the heat-affected zone (HAZ)—the transitional area between the molten weld pool and the unaffected base metal. Since the HAZ does not fully melt, it undergoes structural and mechanical changes due to the rapid and intense thermal cycles experienced during the welding process. (Tadeusz, and Wiktor Wciślik, 2024)

The heat introduced into the welding process and the subsequent re-cooling change the physical properties of the base material, the weld joint, and the HAZ area in particular. The grain size for the simulation was estimated from literature, with the average grain size of ferrite being 25 µm, considering that its volume fraction is 76%. The grain size of the eutectoid ferrite (alpha) and cementite (theta) of the pearlite islands is around 20 µm in the study area CGHAZ – FGHAZ (Coarse Grain - Fine Grain HAZ), where common weld defects, such as cracking, occur after repairs and under temporal stress. The base material grain size is approximately 10 to 25 µm, so we used 25 µm as the largest initial grain size in the simulation. (Li, Wenqiang et al., 2021; Prasanna, N., Anand Ramanathan, and N. Siva Shanmugam, 2023; Pała, Tadeusz, and Wiktor Wciślik, 2024.)

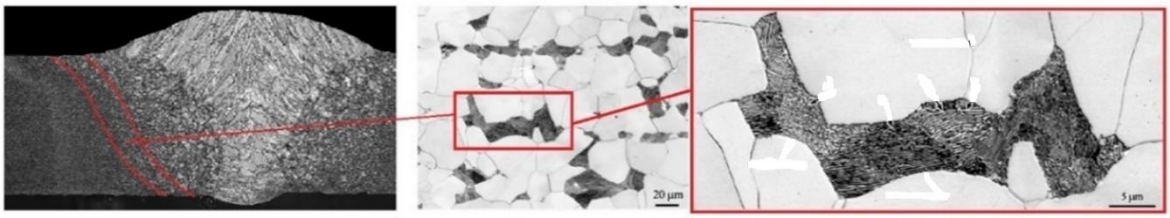

Figure 17. Ferrite grain size (Patrik Klučiar, Igor Barenyi, Jozef Majerík 2022).

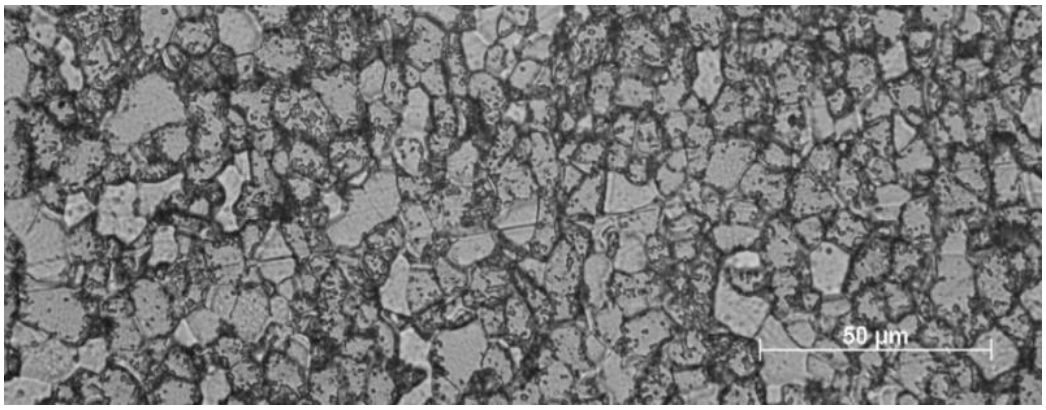

Figure 18. 16Mo3 steel base metal microstructure, grain size ~13µm (Patrik Klučiar, Igor Barenyi, Jozef Majerík 2022).

Heat treatment after welding is performed according to the Welding Procedure Specification (WPS) at 650°C for 3 hours to reduce stresses and minimize distortion in the weld and surrounding areas. The grain size increases by 0.8 microns (figure 21), which is not significant enough to impact grain growth, and therefore, it can be neglected in the simulation.

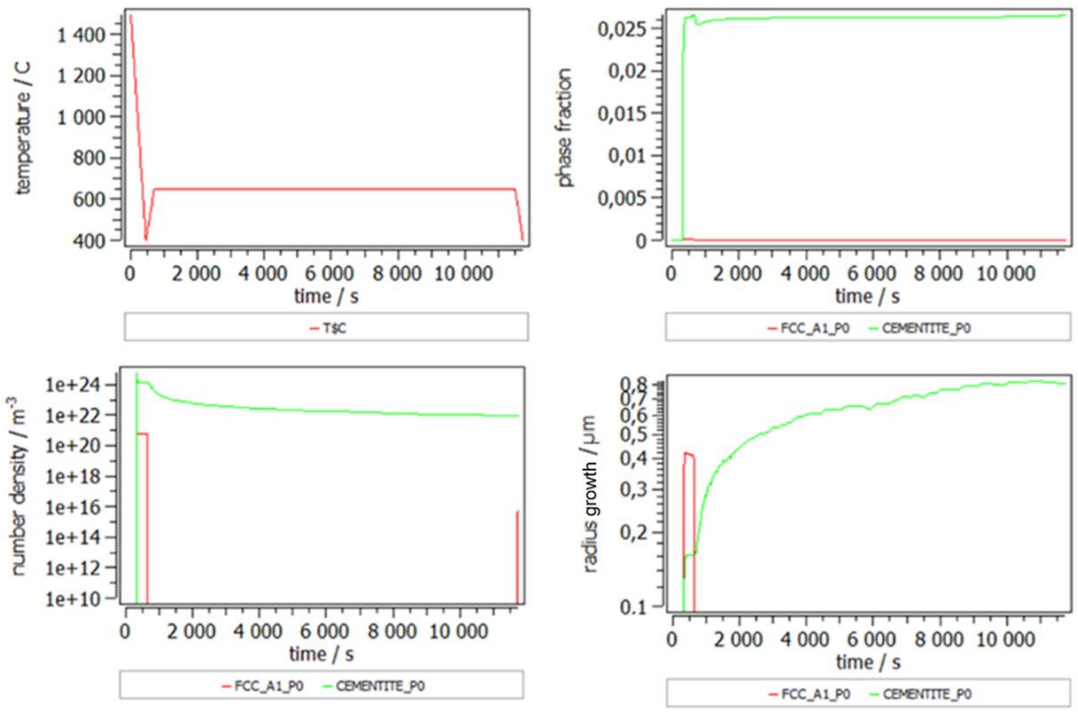

Figure 19. Grain growth after heat treatment 650˚C for 3 hours

The cooling time after welding was calculated mathematically by specifying the t8/5 time (1). Most metallurgical changes occur when the temperature decreases from 800°C to 500°C, a range commonly expressed in terms of t8/5 cooling time. Therefore, the cooling time for this temperature range was calculated using dedicated software. The changes in physical properties are primarily influenced by heat input and cooling time, both of which directly affect the properties of the weld joint.

A high heat input results in a longer cooling time, which increases the size of the Heat-Affected Zone (HAZ) and reduces the joint's durability. Conversely, rapid cooling due to insufficient heat input can lead to defective or weak joints caused by poor weld penetration and incomplete melting of the material. For these reasons, it is crucial to carefully control both heat input and cooling time during welding to achieve an optimal weld.

To initiate the simulation, the 16Mo3 power plant boiler wall material WPS (Attachment “Power plant WPS”) was used to calculate the cooling times. The t8/5 cooling time can be calculated to approximately 125 seconds using the following formula.

Using equation 2 to calculate t8/5 time (Martikainen J. 2015):

$$t_{5/8} = ((6700 - 5 * T_P) * Q * (1/(500-T_P) - (1/(800-T_P) * F_2) * d \quad (2)$$

Where:

T_P = Preheating Temperature ^0C

Q = Heat Input (kJ/mm), $Q = \varepsilon*((V*I*60)/(S*1000))$

ε = Thermal Efficiency of Welding Process

V = Voltage (V)

I = Current (I9

S = Welding Speed (mm/min)

F2 = Welding geometry Factors

d = Plate thickness (mm)

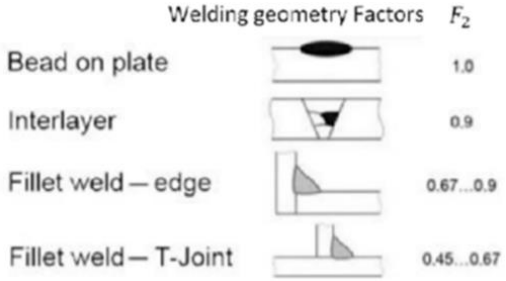

S.N	Welding Process	Thermal Efficiency
1	Submerged Arc Welding (SAW)	1.0
2	Shielded Metal Arc Welding (SMAW)	0.8
3	Gas Metal Arc Welding (GMAW)	0.8
4	Flux Cored Arc Welding (FCAW)	0.8
5	Gas Tungsten Arc Welding (GTAW)	0.6
6	Plasma Arc Welding (PAW)	0.6

Figure 20. Welding geometry factors for calculating t5/8 value.

Or just by using the internet to ~118 seconds:

Table 2. Weld cooling t5/8 time (Migal.co, 2022).

Arc voltage	10,50	Preheat temperature	250,00
Arc current	130,00	Welding process	Tungsten input gas welding (TIG)
Welding speed	3,00	Nahtar	1. and 2. fillet weld on T - or cross joint
Plate tickness	5,00	Calculated energy	E = 2,00 kJ/mm
		Clculated heat input	Q = 1,20 kJ/mm
		Calculated cooling time	t 5/8 = 117,90 s

The temperature changes during the simulated repair welding, from the initial melting of the weld to its subsequent cooling across the material interfaces, were taken into account. These temperature variations influence the phase transitions of the austenitic and ferritic surfaces, and thus, the phase changes were incorporated into the simulation when designing the structure of the model.

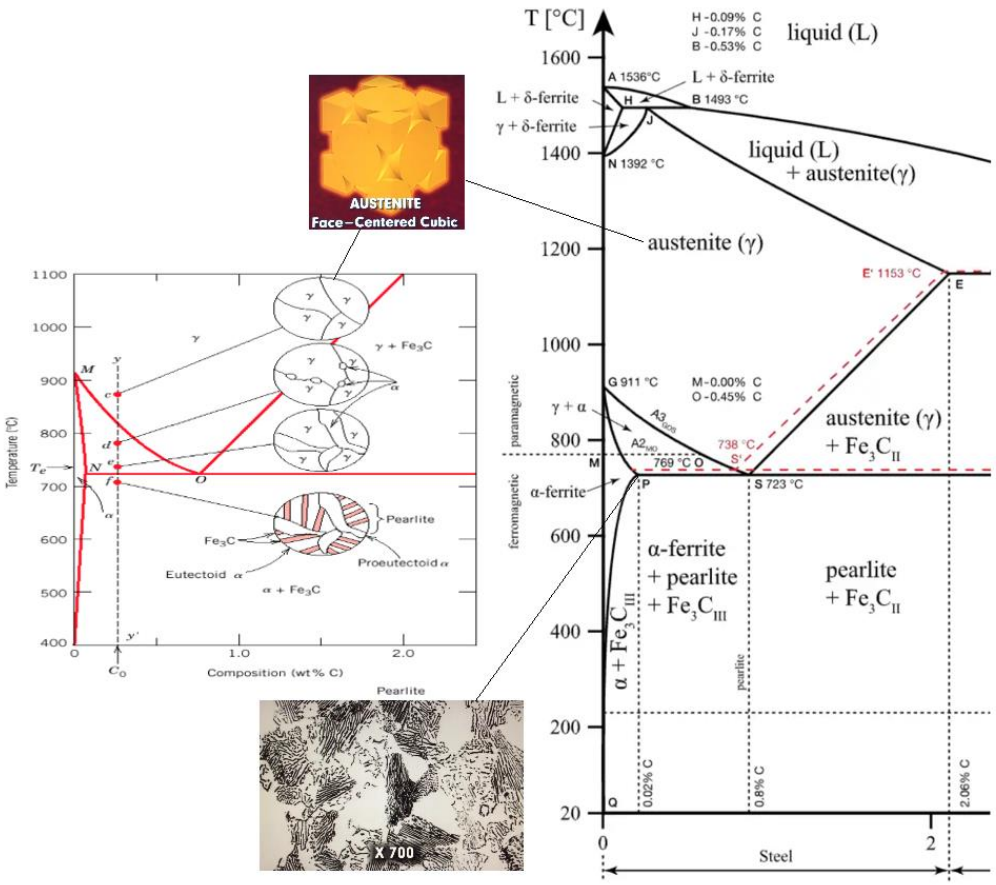

Figure 21. Iron-carbon Fe - C equilibrium diagram ~0,2 % Ferrite 71.4% and 28.6%. Perlite (Saif al-din ali 2018).

This approach allows the simulation of up to three separate repair welding treatments within a single simulation. This is typically the maximum number of repairs that can be made to the same point in a power boiler's service history, without the need to replace the part entirely.

The simulation is structured in MatCalc as follows, defining the simulation boundaries:

Table 7. Simulation temperature boundaries

1 493-720 ˚C > 2,4 ˚C / s asthenic	2. 723-400 ˚C > 2.4 ˚C / s ferrite
3. 400-723 ˚C > 300 ˚C /s weld	4. 723-1490 ˚C > 300 ˚C /s weld
5. 1493-720 ˚C > 2,4 ˚C / s asthenic	6. 723-400 ˚C > 2.4 ˚C / s ferrite
7. 400-723 ˚C > 300 ˚C /s weld	8. 723-1490 ˚C > 300 ˚C /s weld
9. 1493-720 ˚C > 2,4 ˚C / s asthenic	10. 723-400 ˚C > 2.4 ˚C / s ferrite

The final strength of the material after the simulation was determined by calculating the strength of 16Mo3 using the rule of mixtures for phases, considering the strength of each phase. The total strength was then predicted by summing the individual phase strengths based on their respective phase fractions. The strength values for each phase are as follows: austenite 200 MPa, ferrite 300 MPa, and bainite 400 MPa.

Table 3. Strength values for each phase

Austenite (FCC_A1)	0,00252329 * 200MPa	= 0,505 MPa
Ferrite (BCC_A2)	0,972008*300MPa	= 291,602 MPa
Cementite	0,0254684*400MPa	= 10,631 MPa
		tot. 302,738 MPa

Typically, the yield strength of 16Mo3 is around 350 MPa. According to the simulation results, in the examined HAZ area of the weld, the material shows a significant weakening (Table 5), with the strength reduced by 13.7% compared to the original yield strength.

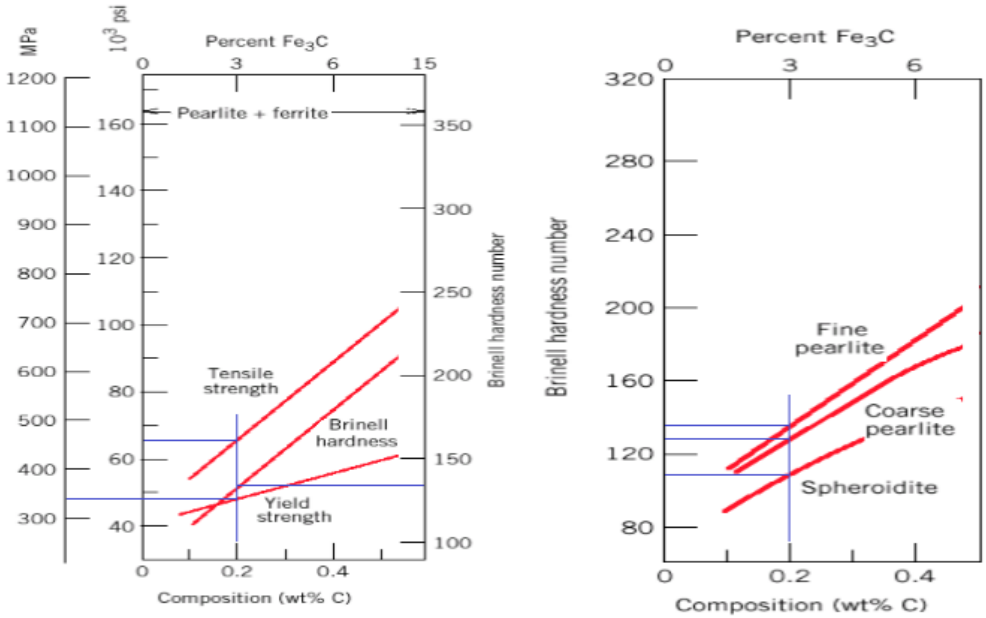

Figure 22. 16Mo3 strength properties

Effects to the HAZ area after three repair welds made the initial grain size to nearly triple it’s size.

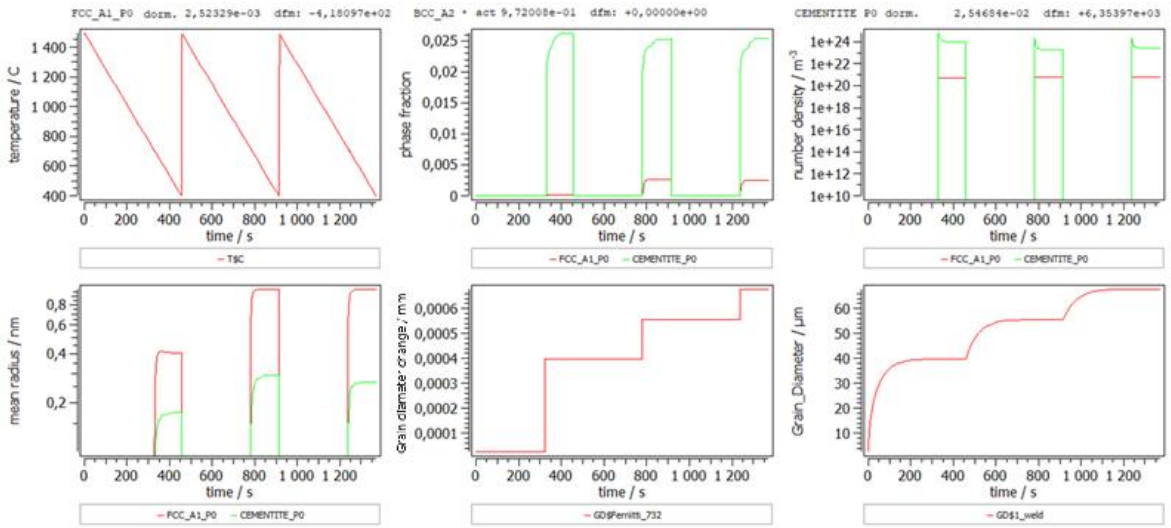

Figure 23. Grain size increase in three repair welds

The weakest point of the entire boiler is most likely the repaired weld HAZ area, which, in practice, is where breakage typically occurs during boiler operation. The grain size in this area ranges from 67.8 µm to a total of 92.8 µm.

The observed grain size increase in repair welding—from 25 µm to 92.8 µm after three welds—represents a notable deviation from standard welding outcomes. This change highlights the sensitivity of the heat-affected zone (HAZ) to thermal cycles during welding. Previous studies confirm that grain growth is significantly influenced by welding parameters, particularly heat input; for instance, a study on conventional austenite with a heat input of Q = 1.0 kJ/mm emphasized this dependency (Kauppi, 2022).

Grain coarsening has also been shown to reduce mechanical properties such as yield strength and impact toughness, ultimately compromising the weld’s overall durability (Kauppi, 2021). The significant grain growth observed in this case may result from several factors, such as a lack of optimization in welding parameters, insufficient preheating, or inadequate post-weld treatments. Such growth can weaken the mechanical properties of the weld and its long-term durability, especially in structures exposed to high temperatures and mechanical loads.

It is recommended to review the welding parameters used, the effects of preheating and post-weld treatments, and the selection of materials for welding. Additionally, the effects of grain growth on the material properties should be thoroughly assessed to ensure sufficient durability of the weld and HAZ in the intended applications.

Some materials in the metal alloy are included primarily due to factors related to casting technology and surface properties. To avoid their interference with the calculation and achieve more accurate results, these materials were intentionally excluded from the simulation.

To simplify the simulation, only the key elements C, Cr, Ni, Mn, Mo, and Si—were considered. Additionally, more phase calculation parameters, such as M23C6, M7C3, and M6C, were incorporated into the simulation using average literature temperatures for each phase's temperature range (Figure A1 in appendices).

After modifying the simulation, the phase composition as a function of temperature and structural content became much clearer, especially when the focus shifted away from the strength property perspective.

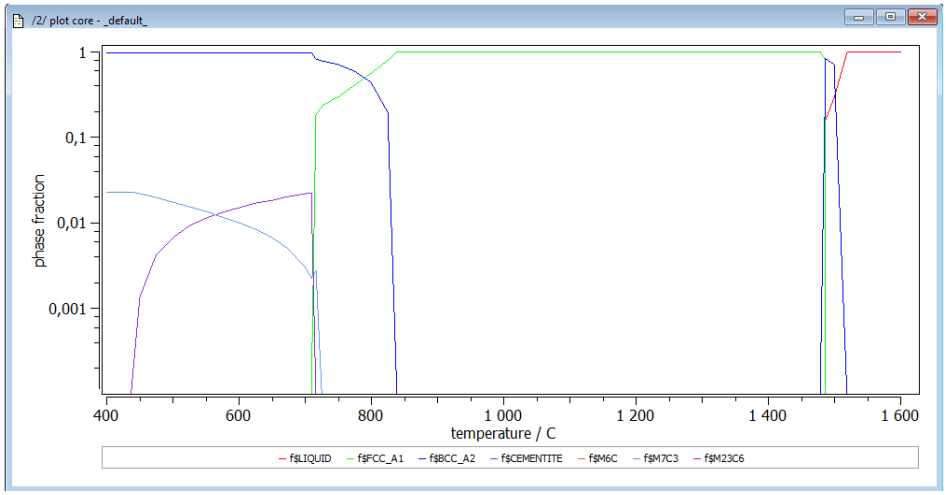

Figure 24. Phase composition in function of temperature and structural content

Each phase was then input into the program as follows:

Liquid phase: 1493–1375°C, first austenite: 1375–1185°C, M6C: 1185–860°C, M7C3: 860–769°C, second austenite: 769–720°C, M23C6: 720–769°C, Ferrite / Bainite: 720–400°C,

(figure A2 and A3 in appendices). (Bogachev, V.A. & Kreitser, K.K. 2022; Armia, Faleri et al. 2020).

The final theoretical strength of 16Mo3 was calculated using the rule of mixtures (figure 29), considering the strength of each phase:

Table 9. Strength values for each phase

Austenite (FCC_A1)	0,00127391 * 200MPa	= 0,255 MPa
Ferrite (BCC_A2)	0,971237*300MPa	= 291,371 MPa
Bainite (Cementite)	0,0274889*400MPa	= 10,996 MPa
		tot. 293,622 MPa

The typical yield strength of 16Mo3 is around 350 MPa. The results from the modified simulation indicate a reduction in strength compared to earlier calculations. This decrease of 16.1% could be due to the exclusion of other materials, which previously contributed to an increase in strength. After simplifying the simulation, the calculated strength is lower than before the modification.

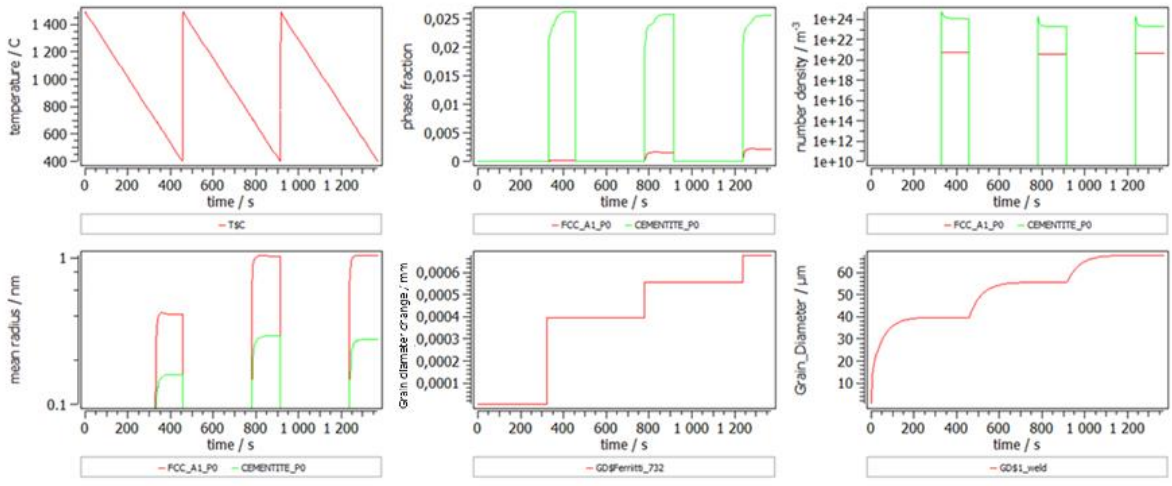

Figure 25. Grain growth with modified materials

Also, the grain growth is a bit stronger (approximately 2,85% effect) 68,3µm to total of 93.3µm.

Grain growth in the heat-affected zone (HAZ) during three repair welds can vary significantly depending on several factors, such as welding parameters, temperature, heat input, and the duration of the welding process. In general, grain growth is observable in repair welding, but it can be more pronounced compared to traditional welding processes due to the repeated and cumulative heat effects.

Several studies suggest that grain growth in repair welding can range from 10-100 µm, depending on the welding parameters and the influence of other factors. After three repair welds, as in the case presented, where the grain size increased from 25 µm to 93.3 µm, this 68.3 µm growth is significant and deviates from standard practices, especially when compared to the changes observed after a single weld (Kawiak and Kochmański, 2024).

At such a growth rate in the HAZ, it is crucial to consider the potential degradation of the material's mechanical properties, such as strength, toughness, and fatigue resistance. Long-term effects can be substantial, especially in structures exposed to repeated loading and high temperatures.

In conclusion, grain growth in the HAZ during repair welding can be significantly greater compared to conventional welding processes, but a precise assessment always depends on the specific process parameters and welding conditions used.

6 Results

Impact of Grain Growth on Weld Durability in Low-Carbon Steel

The growth of grain size in low-carbon steel significantly affects the durability of the weld seam by influencing mechanical properties and failure mechanisms.

Effect on Strength and Toughness - Coarse-Grained Microstructure and Reduced Strength: A finer grain structure enhances strength by introducing more grain boundaries that hinder dislocation movement, as explained by the Hall-Petch relationship. However, as grain size increases, strength decreases. (Kawiak, Michał, and Paweł Kochmański, 2024)

Toughness Reduction: Larger grains make the steel more brittle, facilitating fracture propagation along grain boundaries. This increases the risk of cracking and brittle fracture, particularly at low temperatures or under impact loads.

Effect on Fatigue Resistance of the Weld Joint - Decreased Fatigue Resistance: Areas experiencing significant grain growth in the weld seam, especially in the heat-affected zone (HAZ), become more vulnerable to fatigue damage. Coarse-grained structures are less effective in absorbing stress compared to fine-grained structures.

Effect on Weld Brittle Fracture - Increased Brittleness: Grain growth in the hardened HAZ raises brittleness, particularly when welding at high temperatures, followed by rapid cooling that results in martensitic or bainitic structures. This transformation increases the susceptibility of the weld joint to fracture.

Softening in the HAZ: Excessive grain growth without martensitic transformation can lead to softening, forming a mechanically weak zone where deformations concentrate.

Effect on Weld Crack Susceptibility - Promotion of Hot Cracking: Larger grains can increase the likelihood of hot cracking due to inhomogeneities in the molten zone, fostering the growth of microcracks.

Increased Hydrogen Embrittlement Risk: Coarse grains facilitate hydrogen diffusion and accumulation at grain boundaries, heightening the risk of hydrogen embrittlement, particularly in high-strength steels.

Comparison of Coarse- and Fine-Grained Structures - Coarse-Grained Structures: Weaken strength, toughness, and fatigue resistance. Grain growth in the HAZ can lead to softening, increased brittleness, and higher crack susceptibility.

Fine-Grained Structures: Improve strength and toughness, prevent brittle fracture propagation, and enhance fatigue resistance. They also raise the ductile-to-brittle transition temperature, making the weld more resistant to impact loading at low temperatures.

Welding Techniques: Methods such as preheating and using suitable filler materials help control grain size and improve weld durability.

Evaluation of Repair Welding Effects on the HAZ - A simulation assessed the impact of multiple repair welds on the HAZ of a power boiler over its lifespan. The study examined grain coarsening trends, focusing on the temperature-dependent effects of three consecutive repair welds. The simulation did not account for aging or heat treatment effects that naturally occur over time in service conditions.

The simulated grain growth in the HAZ aligns with literature, which reports a grain size range of approximately 10-100 μm (Kalliokoski J 2013; Mohammadi Zahrani, E, and A.M. Alfantazi, 2021; Kawiak, Michał, and Paweł Kochmański, 2024; Bayraktar, E et al., 2007).

Long-Term Steel Degradation - Steel degradation is inevitable in high-temperature, pressurized systems operating under creep conditions. Over time, coarse grain growth, carbide spheroidization, and in some cases, graphitization occurs, affecting mechanical properties. These changes are particularly relevant for 16Mo3 steel, commonly used in welded structures for power plants operating at elevated temperatures.

Graphitization, predominantly observed in carbon steels such as 16Mo3, is a critical degradation mechanism in high-temperature welded structures, influencing the remaining service life of power plant boilers.

Fracture Toughness and Tensile Strength of Repair Welds - The fracture toughness and tensile strength of repair welds, particularly in the HAZ, are significantly lower than those of the base material. Micro voids and inclusions in the form of fine spheroidal particles

contribute to reduced fracture toughness. However, toughness improves in the HAZ compared to the repair weld itself and is highest in the native material. (Bayraktar, E et al., 2024; Bayraktar, E et al., 2007)

Transformation of Austenite to Ferrite, Cementite, and Pearlite - The transformation of austenite into ferrite, cementite, and pearlite plays a crucial role in shaping the microstructure of carbon steel. When pearlite content exceeds 20%, plasticity and fracture toughness decrease significantly.

Long-term exposure to temperatures around 480°C in steam boilers leads to major microstructural changes in steels. (Kawiak, Michał, and Paweł Kochmański, 2024.)

Simulation Results: Grain Growth and Repair Welds - The simulation results indicate that after three repair welds, the grain size increased nearly fourfold, from 25 µm to 93.3 µm (a 373.2% increase). This growth is independent of normal heat treatment or aging processes, which were not included in the simulation. Typical grain growth due to heat treatment was around 0.8 µm per repair weld. Aging effects were excluded, as they occur gradually over the boiler’s operational life, whereas this study focused on the immediate impact of repair welding within a short timeframe.

7 Discussion

While changes in the properties of the weld seam and the heat-affected zone (HAZ) can be partially mitigated by selecting suitable filler materials and controlling heat input and post-weld heat treatment (PWHT) parameters, it is essential to recognize the significant influence of the welding process on the overall joint properties. The weld area and its surrounding region typically undergo extensive grain growth, which considerably reduces material strength. This effect is particularly pronounced in fine-grained steels, emphasizing the need for precise control and minimization of heat input during welding.

To anticipate the impact on material properties, estimating grain size in the HAZ beforehand is beneficial. This can be achieved through simulations of various temperature cycles, allowing for the assessment of final properties and the implementation of necessary preventive measures and quality checks. Many calculation and simulation programs predict grain size behavior below 1200°C using adjustable equations that account for changes in austenite content. These models analyze the effects of welding on HAZ mechanical properties, often aiming to test specimens under similar conditions to validate and refine welding procedure specification (WPS) values. Our simulation closely matched the physical values reported in the literature, obtained through the analysis and measurement of actual test samples using different manufacturing methods. Consequently, simulating material behavior under similar conditions provides a reliable estimate of the strength characteristics of repair-welded components.

Beyond heat treatment, alternative methods can enhance the strength and toughness of repair welds. Improving steel properties is not solely dependent on welding control and heat treatment applications. For example, surface deformation techniques, such as forging in the repair area, can enhance the toughness, tensile strength, and elongation properties of the HAZ. However, the practicality and cost-effectiveness of such methods depend on the part's location and intended function.

Traditionally, hardness testing of the HAZ and weld metals is conducted manually to quickly assess the actual joint properties without simulations. However, when estimating the properties of future or existing welds without performing the actual work, simulations based on real-world data offer a reliable means of evaluating material properties.

Degradation mechanisms of the HAZ in low-carbon steel welding, experimental studies on the degradation mechanisms in the HAZ of low-carbon steel welding have yielded several key insights:

Microstructural Changes and Mechanical Properties: Heat exposure alters the HAZ microstructure, potentially weakening the mechanical properties of the steel. Heat input during welding and cooling rates significantly influence the size of the HAZ and the resulting grain structure.

Ferrite Content Determination: Techniques have been developed to measure ferrite content in the HAZ using optical metallurgical microscopes. Both manual point counting and image analysis software are employed to assess the base material, weld metal, and HAZ regions, improving measurement repeatability and reducing analysis time.

Fatigue Resistance: The fatigue resistance of fillet weld joints made from different strength classes of steel has been examined through dynamic testing. Findings indicate that the mechanical properties of the HAZ significantly affect weld joint durability under cyclic loading.

These experimental studies highlight the critical role of HAZ microstructure and properties in determining the longevity of welded joints in low-carbon steel. Proper control and management of the HAZ are essential to ensuring the quality, reliability, and durability of welded components, particularly in demanding applications such as power plants (Laitinen, T. 2015; Pelttari, C. 2024; Kosti, M. 2019).

8 Conclusions

16Mo3 is a low-alloy steel containing molybdenum, commonly used in high-temperature applications such as boilers and pressure vessels. It offers good weldability; however, specific precautions must be taken to prevent degradation in the weld and heat-affected zone (HAZ). These precautions include preheating and post-weld heat treatment, particularly for thicker materials.

Potential Degradation Mechanisms in 16Mo3 Steel Welds - Fatigue Damage: Fatigue-related failures are common in welded steel structures. Stress concentration caused by weld geometry and defects increase the risk of crack propagation and eventual fatigue failure.

Hot Cracking: Hot cracking can occur during high-temperature welding, especially when there is a significant mismatch in the thermal expansion coefficients of the filler metal and base material. Improper welding parameters can also contribute to this issue.

Hydrogen Embrittlement: Hydrogen introduced during welding can diffuse into steel, causing brittle fractures, particularly if preheating and post-weld heat treatment are not properly executed.

Although specific images of 16Mo3 weld degradation are not included, welding defects and their mechanisms are well-documented in the literature.

Post-Weld Treatment Methods - High-Frequency Mechanical Impact (HFMI) treatment enhances the fatigue resistance of welded joints, mitigating fatigue-induced degradation in load-bearing components. The use of appropriate filler materials specifically designed for welding 16Mo3 steel is essential. Additionally, adhering to steel-specific guidelines and industry standards for preheating and post-weld heat treatment minimizes the risk of degradation mechanisms. (Leppälä, P. 2023.)

The primary degradation mechanisms in 16Mo3 steel welds—fatigue damage, hot cracking, and hydrogen embrittlement—can be mitigated through proper welding techniques and parameters, ensuring long-term durability and reliability. (Leppälä, P. 2023.)

Cracking Behavior in the Base Material - Cracks in the base material typically propagate outside the centerline of the hardened zone into the annealed area, following the grain

boundaries—a characteristic of heat-hardened materials. The austenite interface contains carbide chains, which can serve as crack initiation points due to increased hardness. Bainite and small amounts of martensite are also present in these regions, leading to what is commonly known as annealing cracking. The extent and impact of this cracking can be accurately predicted using simulation software, as applied in this study.

Grain Growth in the Heat-Affected Zone - Analysis of grain growth in the HAZ of 16Mo3 steel after three repair welds shows an increase from an initial 25μm to 92.8μm. This substantial growth can significantly impact the material's mechanical properties, aligning with findings from metallurgical research on the effects of multiple welding cycles on grain size.

For example, Chen et al. (2015) studied grain growth in the HAZ of 304 stainless steels during multipass welding using Monte Carlo simulations and experimental measurements. Their findings confirmed that repeated welding passes contribute to substantial grain growth, affecting mechanical performance. Similarly, Jamshidi et al. (2009) investigated the effect of heat input on grain growth in gas tungsten arc welding of 304 stainless steel, demonstrating that higher heat inputs led to increased grain size, influencing toughness and strength.

A study by Vitasek (2023) examined the impact of weld repairs on the microstructure and mechanical properties of 16Mo3 steel. It highlighted that multiple repair welds caused grain coarsening in the HAZ, compromising the material's mechanical integrity. Additionally, Fujiwara et al. (2018) proposed a model for predicting austenite grain growth in the HAZ of low-alloy steels, considering alloying elements and welding conditions.

These studies collectively reinforce that the observed grain growth from 25 μm to 92.8 μm after multiple repair welds is consistent with existing research. This grain coarsening can adversely affect mechanical properties, including toughness and strength, emphasizing the need for careful control of welding parameters and repair procedures to maintain material performance.

References

Afonine, Pavel V. ; Moriarty, Nigel W. ; Mustyakimov, Marat ; Sobolev, Oleg V. ; Terwilliger, Thomas C. ; Turk, Dusan ; Urzhumtsev, Alexandre ; Adams, Paul D. “FEM: Feature-Enhanced Map.” Acta crystallographica. Section D, Biological crystallography. 71.3 (2015): Pp.646–666. Web.

Akin, J. E. Finite Element Analysis with Error Estimators : An Introduction to the FEM and Adaptive Error Analysis for Engineering Students. 1st ed. Oxford: Elsevier, 2005.

Armia F, Putra, Teuku E, Husaini, Husaini A, Nurdin A, Akhyar. “Study on Fracture Failures of the Super Heater Water Pipe Boiler.” Diffusion and defect data. Solid state data. Pt. A, Defect and diffusion forum 402 (2020): Pp.20–26. Web.

Arora, P., Singh, P.K., Bhasin, V., Vaze, K.K., Ghosh, A.K., Pukazhendi, D.M., Gandhi, P. & Raghava, G. (2011) 'Predictions for fatigue crack growth life of cracked pipes and pipe welds using RMS SIF approach and experimental validation', The International Journal of Pressure Vessels and Piping, 88(10), pp. 384-394.

Barbosa, C., De Barros, S.K., De Cerqueira Abud, I., Lopes Do Nascimento, J. & Santana De Carvalho, S. (2012) 'Failure analysis of an Aqua Tubular boiler tube', Journal of Failure Analysis and Prevention, 12(6), Pp. 654-659.

Barzin, Behzad. Simulation and Material Calibration of Ultra High Strength Steel (UHSS) S960 Welded Joint under Static Tensile Test Utilizing Finite Element Method (FEM). N.p., 2015. Print.

Bayraktar, E et al. “Grain Growth Mechanism during the Welding of Interstitial Free (IF) Steels.” Journal of materials processing technology 189.1 (2007): Pp.114–125. Web.

Bogachev, V.A. & Kreitser, K.K. (2022) 'Study of the ultimate strength of steel grade X10CrMoVNb9-1 (T91) boiler pipe metal', Power Technology and Engineering, 55(6), pp. Pp.906-909.

Finite element analysis with error estimators an introduction to the FEM and adaptive error analysis for engineering students Akin, J. E. 2005

Finite-element creep damage analyses of P91 pipes, Hyde, T.H.; Becker, A.A.; Sun, W.; Williams, J.A. Inter-national journal of pressure vessels and piping, 2006, Vol.83 (11), Pp..853-863

Ghosh, D., Ray, S., Mandal, J., Mandal, N. & Shukla, A.K. (2018) 'Failure analysis of PRDS pipe in a thermal power plant boiler', Journal of the Institution of Engineers (India) Series C, 99(2), Pp.. 233-238.

HAASE, Ryan J, and Larry D HANKE. "Boiler Stack Economizer Tube Failure." Journal of failure analysis and prevention 13.5 (2013): Pp.513–520. Web.

Hakkarainen, T. (2013) 'Vesihöyrypiirin kiertolaskenta kuplapetikattilassa', Lappeenranta University of Technology, Faculty of Technology, LUT Energy, Energy Technology.

Hyde, T.H et al. "Finite-Element Creep Damage Analyses of P91 Pipes." International journal of pressure vessels and piping 83.11 (2006): Pp.853–863. Web.

Izaki, Toru et al. "A Creep Life Assessment Method for Boiler Pipes Using Small Punch Creep Test." International journal of pressure vessels and piping 86.9 (2009): Pp.637–642. Web.

Jalovaara, J., Aho, J., Hietamäki, E. & Hyytiä, H. (2013) Paras käytettävissä oleva tekniikka (BAT) 5–50 MW:n polttolaitoksissa Suomessa. Suomen Ympäristö. Available at: https://www.motiva.fi/files/8707/Paras_kaytettavissa_oleva_tekniikka_(BAT)_5-50_MWn_polttolaitoksissa_Suomessa.pdf.

Jamshidi Aval, H, S Serajzadeh, and A. H Kokabi. "Prediction of Grain Growth Behavior in HAZ During Gas Tungsten Arc Welding of 304 Stainless Steel." Journal of materials engineering and performance 18.9 (2009): Pp.1193–1200. Web.

Kalliokoski J (2013) 'Materiaalitietokanta terästen mikrorakennekuvien vertailuun. Case: Inspecta Oy' Opinnäytetyö Centria University of vocational school. Available at https://www.theseus.fi/bitstream/handle/10024/68010/Kalliokoski_Jussi.pdf.pdf;jsessionid=46408B56D4DD21FC7C3465A594065BC9?sequence=1

Kauppi T, (2013) ’Korkeiden lämpötilojen teräkset, Sarja B’ , Kemi-Tornio University of Applied Sciences

Kauppi, T. 2021. Käytännön hitsausmetallurgiaa osa 3 : esimerkkejä rakenneterästen käyttäytymisestä sulahitsauksessa. Hitsaustekniikka. 73 (3), Pp.32-37. Available at:https://www.theseus.fi/bitstream/handle/10024/503884/Kaytannon_hitsausmetallurgiaa_osa_3.pdf?sequence=1&utm_source=chatgpt.com

Kauppi, T. 2022. Käytännön hitsausmetallurgiaa osa 6 : raekoko, sen määritys ja merkitys austeniitin hajaantumisessa rakenneterästen hitsauksessa. Hitsaustekniikka. 74 (3), Pp.33-37. Available at:https://www.theseus.fi/bitstream/handle/10024/755959/Kaytannon_hitsausmetallurgiaa_osa_6_raekoko_sen_maaritys_ja_merkitys_austeniitin_hajaantumisessa_rakenneterasten_hitsauksessa.pdf?sequence=1&utm_source=chatgpt.com

Kawiak, Michał, and Paweł Kochmański. “Degradation of the Welded Joint Microstructure of a 40-Year-Old Pressure Vessel Made OF 16Mo3 Steel.” Engineering failure analysis 161 (2024): 108227-. Web.

Kazaryan, A et al. “Grain Growth in Anisotropic Systems: Comparison of Effects of Energy and Mobility.” Acta materialia 50.10 (2002): Pp.2491–2502. Web.

Khedr, M., Abd Elaziem, W., Newishy, M. & Abdel-Aleem, H. (2023) 'Metallurgical analysis of ASME SA213 T12 boiler vertical water-wall tubes failure', Engineering Failure Analysis, 145, p. 107016.

Kosti, M. (2019) Welded high strength steel rectangular hollow section T-joint, bending resistance and rotational stiffness, Häme University of Applied Sciences. Available at: https://www.theseus.fi/bitstream/handle/10024/171332/ONT_Marko_Kosti.pdf.

Kulawinski, Dirk et al. “Isothermal and Thermo-Mechanical Fatigue Behavior of 16Mo3 Steel Coated with High-Velocity Oxy-Fuel Sprayed Nickel-Base Alloy under Uniaxial as Well as Biaxial-Planar Loading.” Journal of materials research 32.23 (2017): Pp.4411–4423. Web.

Kurek, Andrzej. “Using Fatigue Characteristics to Analyse Test Results for 16Mo3 Steel under Tension-Compression and Oscillatory Bending Conditions.” Materials 13.5 (2020): Pp.1197-. Web.

Laitinen, T. (2015) Effects of welding methods and high strength steels on the fatigue strength of fillet welded joints, Savonia University of Applied Sciences Thesis. Available at: https://www.theseus.fi/bitstream/handle/10024/87018/Laitinen_Tuomas.pdf.

Lathrop Trotter's blog post, 2020, How Boiler Corrosion Occurs and How to Deal With It, Available at: https://xmpro.com/wp-content/uploads/2020/04/8.jpg.

Leckner, Bo, and Fredrik Lind. “Combustion of Municipal Solid Waste in Fluidized Bed or on Grate – A Comparison.” Waste management (Elmsford) 109 (2020): Pp.94–108. Web.

Leppälä, P. (2023) Effect of HFMI-treatment on weld quality and fatigue strength, Lappeenranta–Lahti University of Technology LUT. Available at: https://lutpub.lut.fi/bitstream/handle/10024/165499/Kandidaatintyo_Leppala_Pyry.pdf.

Li, Lifeng et al. “The Impact of Weld Repairs on the Microstructure and Mechanical Integrity of X80 Pipelines in Oil and Gas Transmission.” Processes 13.2 (2025): Pp.512-. Web.

Li, Wenqiang et al. “Strain Gradient Induced Grain Refinement Far below the Size Limit in a Low Carbon Hypoeutectoid Steel (0.19 Wt% C) via Pipe Inner Surface Grinding Treatment.” Journal of materials science & technology 78 (2021): Pp.155–169. Web.

Liu, G. R, H Nguyen-Xuan, and T Nguyen-Thoi. “A Theoretical Study on the Smoothed FEM (S-FEM) Models: Properties, Accuracy and Convergence Rates.” International journal for numerical methods in engineering 84.10 (2010): Pp.1222–1256. Web.

Liu, G.R., Nguyen-Xuan, H. & Nguyen-Thoi, T. (2010) 'A theoretical study on the smoothed FEM (S-FEM) models: Properties, accuracy and convergence rates', International Journal for Numerical Methods in Engineering, 84(10), pp. Pp.1222-1256.

Martikainen J. (2015) 'BK20A2400 Materials and Welding Metallurgy material' and study work I made’

Mohammadi Zahrani, E, and A.M Alfantazi. “Hot Corrosion of Inconel 625 Wrought Alloy and Weld Overlay on Carbon Steel by Gas Metal Arc Welding in 47 PbSO4-23 ZnO-13 Pb3O4-7 PbCl2-5 CdO-5 Fe2O3 Molten Salt Mixture.” Corrosion science 183 (2021): 109348-. Web.

Migal.co, High-quality welding consumables and related technologies, 2022, Available at:https://www.migal.co/index.php?id=124&L=0.

Moravec, Jaromir et al. “Determination of Grain Growth Kinetics and Assessment of Welding Effect on Properties of S700MC Steel in the HAZ of Welded Joints.” Metals (Basel) 9.6 (2019): Pp.707-. Web.

Nonaka, I., Ito, T., Ohtsuki, S. & Takagi, Y. (2001) 'Performance of repair welds on aged 2.25Cr–1Mo boiler header welds', International Journal of Pressure Vessels and Piping, 78(11), Pp. 807-811.

Pała, Tadeusz, and Wiktor Wciślik. “Strength and Fracture Toughness of TIG- and Laser-Welded Joints of Low Carbon Ferritic Steels.” Materials 17.16 (2024): 3956-. Web.

Patrik Klučiar, Igor Barenyi, 2022, Jozef Majerík, Nanoindentation Analysis of Inconel 625 Alloy Weld Overlay on 16Mo3 Steel, Available at: https://journalmt.com/pdfs/mft/2022/01/13.pdf.

Pelttari, C. (2024) Verification and commissioning of the ferrite content measurement with image analysis software, Tampere University of Applied Sciences. Available at: https://www.theseus.fi/bitstream/handle/10024/854590/Pelttari_Carita.pdf.

Prasanna, N, Anand Ramanathan, and N Siva Shanmugam. “Investigation of Welding of Dissimilar High Thickness SA106 Gr.C Carbon Steel and SA335P12 Alloy Steel to Eradicate the Failure in Boiler Components Fabricated through SAW and SMAW Processes.” Engineering failure analysis 149 (2023): 107252-. Web.

Reda, R., Magdy, M. & Rady, M. (2020) 'Ti–6Al–4V TIG weld analysis using FEM simulation and experimental characterization', Iranian Journal of Science and Technology, Transactions of Mechanical Engineering, 44(3), Pp. 765-782.

Reda, Reham, Mohamed Magdy, and Mohamed Rady. “Ti–6Al–4V TIG Weld Analysis Using FEM Simulation and Experimental Characterization.” Iranian journal of science and technology. Transactions of mechanical engineering 44.3 (2020): Pp.765–782. Web.

Richard Rennie, and Jonathan Law. “FEM.” A Dictionary of Chemistry 2020: n. pag. Print.

Saif al-din ali, Iron Carbon Phase Diagram, 2018, Available at:https://www.slideshare.net/slideshow/iron-carbon-phase-diagram-90323001/90323001.

Seki, Akira, and Naoto Fujiyama. “Austenite Grain Growth Simulation in Welding Heat-Affected Zone.” Materials science forum 941 (2018): Pp.620–626. Web.

Shu ZHOU, Ke ZHANG, Nailu CHEN, Jianfeng and Yonghua RONG, "Investigation on High Strength Hot-rolled Plates by Quenchingpartitioning-tempering Process Suitable for Engineering", ISIJ International, Vol. 51 (2011), No. 10, Pp. 1688–1695

Sikanen, T. (2019) (n.d.) (2019) 'Voimakattilaprojektien kustannusrakenne ja markkinahinnan muodostuminen', Diplomityö.

Silva, Lucas Filipe Martins da, Reza Beygi, and Eduardo Cesar Marques. Computational Concepts in Simulation of Welding Processes. Cham, Switzerland: Springer, 2022. Print.

Souza, Gilberto Francisco Martha de, and SpringerLink. Thermal Power Plant Performance Analysis. London: Springer London, 2012. Web.

Tanja Winqvist, Johanna Tuiremo, Hitsaustekniikka 5, 2017, available at:https://www.kiwa.com/fi/fi/uutiset/voimalaitosten-korkean-lampotilan-komponenttien-virumisen-hallinta/.

Var-nosfaderani, M.A., Eslami, A., Saiedi, N. & Bahrami, A. (2019) 'Metallurgical aspects of a blowdown pipe failure in a petrochemical plant', Engineering Failure Analysis, 98, pp. Pp.141-149.

XMPro's official website, 2020, Picture of a damaged boiler. Available at: https://xmpro.com/wp-content/uploads/2020/04/8.jpg

Appendix 1. Power-plant WPS for 16Mo3

Kvaerner Power	WELDING PROCEDURE SPECIFICATION-HITSAUSOHJE - SVETSPROCEDUR SPECIFIKATION (EN 288-2)	WPS- 1268 - T	Muut - Rev 01

PARENT METALS-PERUSAINEET-GRUND MATERIAL

Group-Ryhmä-Grupp	Type or Grade e.g.-Nimike esim.-Specifikation t.ex.
1 1.2Mo	15Mo3, 16Mo3
2 1.2Mo	15Mo3, 16Mo3
1.1ReH<=265N/mm2	P265GH, St 45.8

Standard(s)-Sovellutusstandardi(t)-Standard(er): EN 288-3

Impact test: ☐ No ☒ Yes

WPARs: 1268-T, E400-11-202

PARENT METAL THICKNESS-AINEENPAKSUUS-TJOCKLEK (mm)

Butt Joint-Päittäisliitos-Stumsvets		Branch Connection-Haaraliitos-Rörknut		Fillet Weld-Pienahitsi-Kälsvets (FW)
Groove-Päittäin-Stumsvets (BW)	T-Butt Joint-T-Liitos-T-fog (TBW)	Main Pipe-Pääputki-Huvudrör (BCWI)	Branch Pipe-Yhdeputki-Grenrör (BCWO)	
3.0 - 8.6	3.0 - 8.6	NA	NA	NA

PIPE DIA-PUTKEN HALK.-ROR DIA (mm)

Pipe-Putki-Rör	Braach Pipe-Haaraputki-Grenrör
21.0 - 44.9	NA

ANGLE OF BRANCH CONNECTION-PUTKEN HAARALIITOKSEN KULMA-VINKEL HOS RÖRKNUT: NA °

FILLET WELD THROAT THICKNESS (mm)-PIENAHITSIN a- MITTA-a-MÄTTET AV KÄLSVETSEN: NA

WELDING POSITION-HITSAUSASENTO-SVETSLÄGE: H-L045, PA, PC, PF

JOINT SKETCH-LIITOSKUVA-FOGUTFORMNING

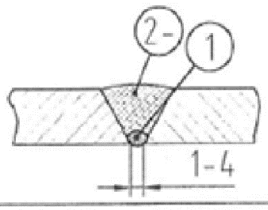

Other joint designs for production, see fabrication drawing
Muut tuotantoraiion muodot, katso valmistuspiirustusta -
Andra fogutformningar i produktion, se tillverkningsritning

PREHEAT-ESIKUUMENNUS-ARBETSTEMPERATUR

Minimi - Min.: 10 °C
Interpass temperature-Palkojen välinen lämpötila-Mellanträngstemperatur Max.: 250 °C

PWHT-LÄMPÖKÄSITTELY-VÄRMEBEHANDLING

Temperature-Pitolämpötila-Temperatur: ☒ No ☒ Yes 550 - 630 °C
See-Katso-Se

WELDING CONSUMABLES-HITSAUSAINEET-TILLSATSMATERIAL

Process-Prosessi-Metod	Filler Metal-Lisäaine-Tillsatsmaterial: Manufacturer/ trade name-Valmistaja/ kaupanimi-Tillverkare/ handelsnamn	Standard/ designation -Standardi/ merkintä-Standard/ beteckning	Welding gas/ flux-Hitsauskaasu/ -jauhe-Skyddsgas/ Pulver: Manufac / trade name-Valm/ kaup-parlim-Tillverkare/ handelsnamn	Stand / design.-Standl merk.-Stand / beteckn	Gas flow-Kaasunvirt.-Flodeshast (l/min)
141	Esab OK Tigrod 13.09	EN 12070 : W MoSi	AGA MISON Ar	EN 439 : I1	10 - 18
141	Böhler DMo-IG	EN 12070 : W MoSi	AGA MISON Ar	EN 439 : I1	10 - 18
Backing gas-Juurikaasu-Skyddsgasen på rotsidan			NA		NA

TECHNIQUE-TEKNIIKKA-TEKNIK

Process-Prosessi-Metod	Stand off distance-Vapaalanganpituus-Avstånd kontaktrör (mm)	Single-(A) Multi pass (B)-Yksi- (A) Monipalko (B)-Enkel- (A) Flersträng (B)	Number of wire electrodes-Lankojen lukumäärä-Antal trådelektroder	Wire feed speed (cm/min)-Langansyöttönopeus-Trådmatningshastighet	Backing-Juurituki-Rotstöd: No-Ei-Nej	Yes-Kyllä-Ja	Back gouging-Juuren avaus-Rotmejsling: No-Ei-Nej	Yes-Kyllä-Ja
141	NA	B	NA	NA	☒	☐	☒	☐
					☐	☐	☐	☐
					☐	☐	☐	☐

MODE OF METAL TRANSFER-AINEENSIIRTYMÄ-TYP AV METALLÖVERFÖRING: Spray arc-Kuumakaari-Spray båge ☐ Globular arc-Sekakaari-Globulär båge ☐ Short circuting arc-Lyhytkaari-Kort båge ☐

TUNGSTEN ELECTRODE-VOLFRAMIELEKTRODI-WOLFRAMELEKTROD Size-Koko-Dia (mm): ∅ 2.4 Identification-Tunnus-Beteckning (EN 26848): WT-20

WELDING DETAILS-HITSAUKSEN SUORITUSARVOT-SVETSDATA

Layer(s)-Palko-keros-Sträng	Process-Prosessi-Metod	Filler metal-Lisäaine-Tillsatsmat. Size (mm)-Halkaisija-Diameter	Electrical parameters-Virta-arvot-Elektriska parametrar: AC/DC +/-	Amperage-Hitsausvirta-Ström	Voltage-Jännite-Spänning	Travel speed-Kuljetusnopeus-Framförings-hastighet (cm/min)	Heat input-Lämmöntuonti-Värmetillförsel (K/mm)	Weaving-Hitsauksen leviys-Pending: No-Ei-Nej	Yes-Kyllä-Ja	(mm)	Dwell Time (s)-Pysäytysaika-Hålltid
1-	141	2.0	DC-	85-150	12 - 17	2.0 - 5.0	>=0.7		X	0.0 - 4.0	NA
1-	141	2.4	DC-	95-165	13 - 18	3.0 - 7.0	>=0.7		X	0.0 - 5.0	NA

REMARKS-HUOM.-ANMÄRKNINGAR

GENERAL REQUIREMENTS-YLEISOHJEET-SVETSNING ALMÄNNA KRAV FS 3-003

Rev.	Manufacturer / Preparer - Valmistaja / Laatija - Tillverkare / Preparerare	Signature-Allekirjoitus-Namnteckning	Date-Päiväys-Datum
01	Kvaerner Power [redacted]	[redacted] Main Welding Co-ordinator	[redacted]

Phase:
M23C6
Constituents:
: CO,CR,FE,MN,NI,V : CO,CR,FE,MN,MO,NI,V,W : B,C% : !
Comment:
Face-centered cubic Cr-rich carbide, can contain significant amounts of W, Mo, V, Ni. Has a large crystallographic unit cell. Common equilibrium carbide in 9-12 mass.% Cr-steels. Precipitation predominantly on prior austenite grain boundaries and lath boundaries.

Phase:
CEMENTITE
Constituents:
: AL,CO,CR,CU,FE%,MN,MO,NB,NI,SI,V,W : B,C%,N : !
Comment:
(Fe,M)C3; orthorhombic. Unit cell consists of four formula units. In particular Cr and Mn can dissolve into cementite in large quantities. W, V, Mo with limited solubilities.

Phase:
M7C3
Constituents:
: CO,CR,FE,MN,MO,NI,SI,V,W : C : !
Comment:
Trigonal Cr-rich carbide with a large crystallographic unit cell. In particular Fe- and Mn-solubilities.

Phase:
M6C
Constituents:
: CO,CR,FE%,MO,V,W : CO,CR,FE,MO,NI,SI,V,W : CO,FE,MO,NI,SI,V,W : C%,N : !
Comment:
Mo,W-rich carbide, can contain significant amounts of Cr and V. Equilibrium phase in steels with relatively low Cr contents. Has a large unit cell. Precipitation predominantly on grain boundaries, also on lath boundaries and prior austenite grain boundaries. M6C#01 is Si-rich nitride Cr3Ni2SiN. Precipitates in some Si- and N-containing stainless steels after long-term aging. □

Figure A1. Explanations of abbreviations from the MatCalc program

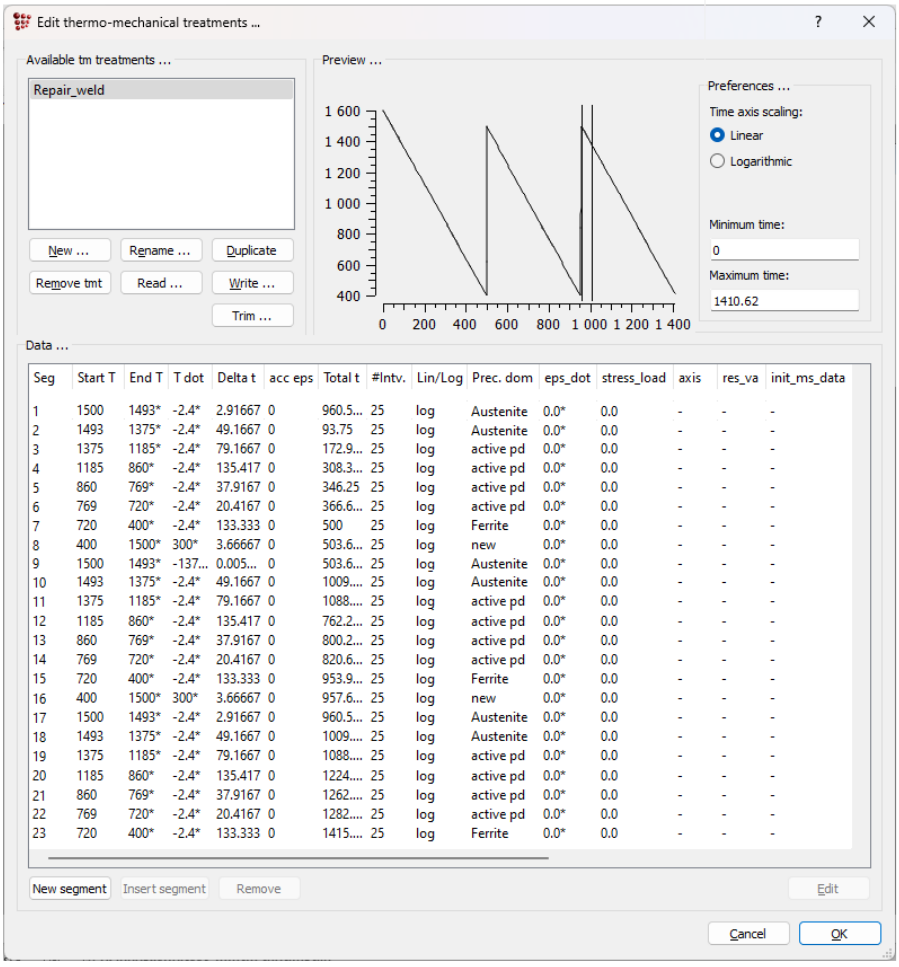

Figure A2. New repair weld boundaries for the simulation.

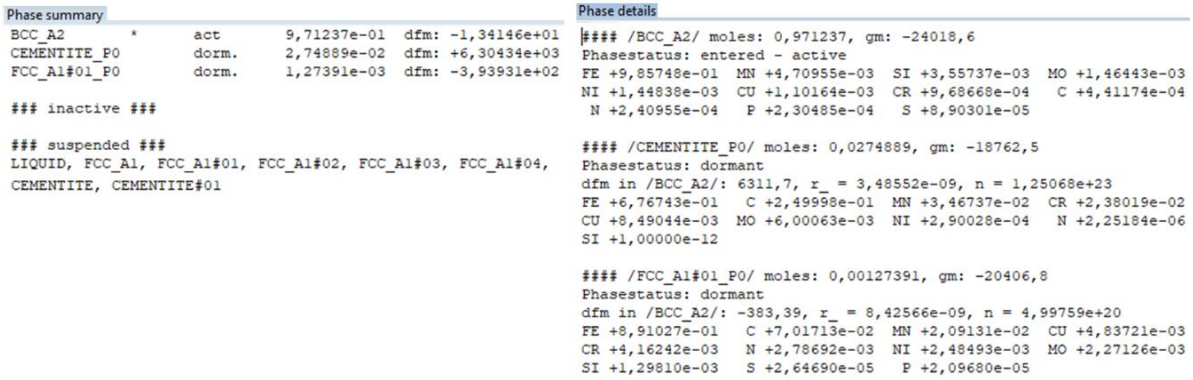

Phase summary

```
BCC_A2          *       act         9,71237e-01   dfm: -1,34146e+01
CEMENTITE_P0            dorm.       2,74889e-02   dfm: +6,30434e+03
FCC_A1#01_P0            dorm.       1,27391e-03   dfm: -3,93931e+02

### inactive ###

### suspended ###
LIQUID, FCC_A1, FCC_A1#01, FCC_A1#02, FCC_A1#03, FCC_A1#04,
CEMENTITE, CEMENTITE#01
```

Phase details

```
#### /BCC_A2/ moles: 0,971237, gm: -24018,6
Phasestatus: entered - active
FE +9,85748e-01  MN +4,70955e-03  SI +3,55737e-03  MO +1,46443e-03
NI +1,44838e-03  CU +1,10164e-03  CR +9,68668e-04   C +4,41174e-04
 N +2,40955e-04   P +2,30485e-04   S +8,90301e-05

#### /CEMENTITE_P0/ moles: 0,0274889, gm: -18762,5
Phasestatus: dormant
dfm in /BCC_A2/: 6311,7, r_ = 3,48552e-09, n = 1,25068e+23
FE +6,76743e-01   C +2,49998e-01  MN +3,46737e-02  CR +2,38019e-02
CU +8,49044e-03  MO +6,00063e-03  NI +2,90028e-04   N +2,25184e-06
SI +1,00000e-12

#### /FCC_A1#01_P0/ moles: 0,00127391, gm: -20406,8
Phasestatus: dormant
dfm in /BCC_A2/: -383,39, r_ = 8,42566e-09, n = 4,99759e+20
FE +8,91027e-01   C +7,01713e-02  MN +2,09131e-02  CU +4,83721e-03
CR +4,16242e-03   N +2,78692e-03  NI +2,48493e-03  MO +2,27126e-03
SI +1,29810e-03   S +2,64690e-05   P +2,09680e-05
```

Figure A3. Phases in mathematical presentation after modification